Stability Analysis for Incremental Nonlinear Dynamic Inversion Control

Wang, Xuerui; van Kampen, Erik-Jan; Chu, Qiping; Lu, Peng

Stability Analysis for Incremental Nonlinear Dynamic Inversion Control

Xuerui Wang,* Erik-Jan van Kampen,† and Qiping Chu‡
Delft University of Technology, 2629 HS Delft, The Netherlands
and
Peng Lu§
Hong Kong Polytechnic University, Hung Hom, Hong Kong, People's Republic of China

As a sensor-based control method, incremental nonlinear dynamic inversion (INDI) has been applied to various aerospace systems and has shown desirable robust performance against aerodynamic model uncertainties. However, its previous derivation based on the time scale separation principle has some limitations. There is also a need for stability and robustness analysis for INDI. Therefore, this paper reformulates the INDI control law without using the time scale separation principle and generalizes it for systems with arbitrary relative degree, with consideration of the internal dynamics. The stability of the closed-loop system in the presence of external disturbances is analyzed using Lyapunov methods and nonlinear system perturbation theory. Moreover, the robustness of the closed-loop system against regular and singular perturbations is analyzed. Finally, this reformulated INDI control law is verified by a Monte Carlo simulation for an aircraft command tracking problem in the presence of external disturbances and model uncertainties.

I. Introduction

NONLINEAR dynamic inversion (NDI) is a nonlinear control approach that cancels the system nonlinearity by means of feedback, which results in entirely or partly linearized closed-loop system dynamics, to which conventional linear control techniques can then be applied [1,2]. This method is essentially different from the widely used Jacobian linearization around specific operating points in combination with gain-scheduled linear controllers, whose stability and performance become questionable between operational points. To achieve an exact dynamic cancellation, the NDI control method requires an accurate knowledge of the nonlinear system dynamics. Such a requirement is almost impossible to meet in reality due to model simplifications, computational errors, and external disturbances. This main drawback of NDI motivated many control technologies to improve its robustness. One popular approach is combining NDI with linear robust control techniques such as structural singular value μ analysis [3,4] and $\mathcal{H}_\infty$ synthesis. Although these techniques have brought benefits to regular NDI, not all the uncertainties are taken into account, or some known nonlinear time-varying dynamics are treated as uncertainties [5]. Therefore, the closed-loop systems can be either marginally or overly conservative in performance and stability robustness [5]. There also exist many attempts at using indirect adaptive control methods to improve the robustness of NDI [6]. Indirect adaptive control methods, in some form or the other, rely on online identification, which requires online excitations and selection of

thresholds. However, the stability of indirect adaptive NDI is not guaranteed [6,7].

Incremental nonlinear dynamic inversion (INDI) is a sensor-based control method, which requires less model information in both qualitative and quantitative senses, thus improving the system robustness against model uncertainties. The concept of this method originates from the late 1990s and was previously referred to as simplified NDI [8] and modified NDI [9]. INDI control has been elaborately applied to various aerospace systems [7,10–22]. Regarding its applications on aerospace systems, the INDI method was normally used for the inner-loop angular rate control [7,10–12,18–20,23], where the relative degree for each control channel equals 1. The internal dynamics are then avoided by using a cascaded control structure, which is a common practice in flight control system designs [7,11,14,18–20]. However, the stability of cascaded control structures is not easy to prove because of its dependency on the time scale separations between different control loops. Also, this cascaded control structure is unsuitable for some problems. For example, it is neither physically meaningful nor practical to separate the higher-order aeroelastic dynamics into cascaded loops.

The existing derivations of the INDI control law are based on the so-called time scale separation principle, which is actually different from the widely used separations based on singular perturbation theories. In [7,10–20], this separation concept was claimed as the controls can change significantly faster than the states. The nonlinear dynamic equations describing the plant dynamics are then simplified into linear incremental dynamic equations by omitting state-variation-related terms and higher-order terms in their Taylor series expansions, based on which the incremental control inputs are designed. This approach is not mathematically rigorous because the plant simplification is made before introducing the INDI control inputs and thus becomes deficient for unstable plants. Moreover, although the state-variation-related terms and higher-order terms are not used in the INDI controller design, they should be kept in the closed-loop dynamic equations and remain influencing the closed-loop system stability and performance, which is also not the case in the literature.

Furthermore, despite the numerically verified robustness of INDI to aerodynamic model uncertainties [10,15,21] and disturbances [13–15,21], its previous theoretical stability and robustness proofs have some drawbacks. These previous attempts drew the stability conclusions based on the linear transfer functions derived from block diagrams [10,13,14], where inappropriate assumptions are made.

---

*Ph.D. Candidate, Control and Simulation Section, Faculty of Aerospace Engineering, Kluyverweg 1; X.Wang-6@tudelft.nl.
†Assistant Professor, Control and Simulation Section, Faculty of Aerospace Engineering, Kluyverweg 1; E.vanKampen@tudelft.nl. Member AIAA.
‡Associate Professor, Control and Simulation Section, Faculty of Aerospace Engineering, Kluyverweg 1; Q.P.Chu@tudelft.nl. Member AIAA.
§Assistant Professor, Interdisciplinary Division of Aeronautical and Aviation Engineering; peng.lu@polyu.edu.hk.

The influences of disturbances and uncertainties on the internal dynamics also remain unknown in the literature.

In this paper, the INDI control in the literature is reformulated for systems with arbitrary relative degree, without using the time scale separation principle. The stability and robustness of the reformulated INDI is then analyzed using Lyapunov-based methods. Finally, this reformulated INDI is compared with NDI both analytically and numerically, considering model uncertainties and external disturbances.

This paper is structured as follows. Section II reformulates the INDI control law for three different problems. The stability and robustness issues of INDI are discussed in Sec. III. The effectiveness of the reformulated INDI is numerically verified in Sec. IV. Main conclusions are presented in Sec. V.

II. Reformulations of Incremental Nonlinear Dynamic Inversion

In this section, the incremental nonlinear dynamic inversion (INDI) control method will be reformulated for three problems, namely the input–output linearization, output tracking, and input-to-state linearization in the presence of external disturbances.

A. Input–Output Linearization

Consider a multi-input/multi-output nonlinear system described by

$$\dot{x} = f(x) + G(x)u$$
$$y = h(x) \tag{1}$$

where $f: \mathbb{R}^n \to \mathbb{R}^n$ and $h: \mathbb{R}^n \to \mathbb{R}^p$ are smooth vector fields. G is a smooth function mapping $\mathbb{R}^n \to \mathbb{R}^{n\times m}$, whose columns are smooth vector fields. When $p < m$, which means that the number of outputs is smaller than the number of inputs, control of this system via input–output linearization is an overdetermined problem, where a control allocation technique is needed. On the other hand, $p > m$ yields an underdetermined problem. Although a weighted least-squares method can be used to solve underdetermined problems, the desired control aims cannot be fully achieved. $p = m$ is assumed in the following derivations.

Denote the elements of h as h_i, $i = 1, 2, \ldots, m$, and the column vectors of the matrix G as g_j, $j = 1, 2, \ldots, m$. Then, the Lie derivatives [2] of the function h_i with respect to the vector fields f and g_j are defined as

$$\mathcal{L}_f h_i = \frac{\partial h_i}{\partial x} f, \qquad \mathcal{L}_{g_j} h_i = \frac{\partial h_i}{\partial x} g_j,$$
$$\mathcal{L}_f^k h_i = \frac{\partial(\mathcal{L}_f^{k-1} h_i)}{\partial x} f, \qquad \mathcal{L}_{g_j} \mathcal{L}_f^k h_i = \frac{\partial(\mathcal{L}_f^k h_i)}{\partial x} g_j \tag{2}$$

The relative degree ρ_i for each output channel i is defined as the smallest integer such that, for all $x \in \mathbb{R}^n$, at least one $j \in \{1, 2, \ldots, m\}$ satisfies $\mathcal{L}_{g_j} \mathcal{L}_f^{\rho_i-1} h_i \neq 0$.

Define the vector relative degree [24] of the system as $\rho = [\rho_1, \rho_2, \ldots, \rho_m]^T$, which satisfies

$$\rho = \|\rho\|_1 = \sum_{i=1}^{m} \rho_i \leq n \tag{3}$$

then the output dynamics of the system can be represented as

$$\begin{bmatrix} y_1^{(\rho_1)} \\ y_2^{(\rho_2)} \\ \vdots \\ y_m^{(\rho_m)} \end{bmatrix} = \begin{bmatrix} \mathcal{L}_f^{\rho_1} h_1(x) \\ \mathcal{L}_f^{\rho_2} h_2(x) \\ \vdots \\ \mathcal{L}_f^{\rho_m} h_m(x) \end{bmatrix}$$
$$+ \begin{bmatrix} \mathcal{L}_{g_1}\mathcal{L}_f^{\rho_1-1} h_1(x) & \mathcal{L}_{g_2}\mathcal{L}_f^{\rho_1-1} h_1(x) & \cdots & \mathcal{L}_{g_m}\mathcal{L}_f^{\rho_1-1} h_1(x) \\ \mathcal{L}_{g_1}\mathcal{L}_f^{\rho_2-1} h_2(x) & \mathcal{L}_{g_2}\mathcal{L}_f^{\rho_2-1} h_2(x) & \cdots & \mathcal{L}_{g_m}\mathcal{L}_f^{\rho_2-1} h_2(x) \\ \vdots & \vdots & & \vdots \\ \mathcal{L}_{g_1}\mathcal{L}_f^{\rho_m-1} h_m(x) & \mathcal{L}_{g_2}\mathcal{L}_f^{\rho_m-1} h_m(x) & \cdots & \mathcal{L}_{g_m}\mathcal{L}_f^{\rho_m-1} h_m(x) \end{bmatrix} u \tag{4}$$

or

$$y^{(\rho)} = \alpha(x) + \mathcal{B}(x)u \tag{5}$$

If $\rho = n$, then the system given by Eq. (1) is full-state feedback linearizable. Otherwise, there are $n - \rho$ internal dynamics unobservable from the output y. According to the Frobenius theorem [25], $\forall\, x_* \in \mathbb{R}^n$, there exist smooth functions $\phi(x) = [\phi_1(x), \phi_2(x), \ldots, \phi_{n-\rho}(x)]^T$ defined in a neighborhood D_0 of x_* such that

$$\frac{\partial \phi_k}{\partial x} g_j(x) = 0, \quad \forall\, k \in \{1, 2, \ldots, n - \rho\}, \quad \forall\, j \in \{1, 2, \ldots, m\},$$
$$\forall\, x \in D_0 \tag{6}$$

Also, $z = T(x)$ defined by

$$z = T(x) = [T_1(x); T_2(x)] = [\eta; \xi], \quad \eta = \phi(x), \quad \xi = [\xi_1; \xi_2; \ldots; \xi_m],$$
$$\xi_i = \left[h_i(x), \mathcal{L}_f h_i(x), \ldots, \mathcal{L}_f^{\rho_i-1} h_i(x) \right]^T, \quad i = 1, 2, \ldots, m \tag{7}$$

is a diffeomorphism on the domain D_0 [2,25]. η and ξ are the state vectors for the internal and external dynamics, respectively. Using Eqs. (5–7), the nonlinear system described by Eq. (1) can be transformed into

$$\dot{\eta} = f_0(\eta, \xi) = \frac{\partial \phi}{\partial x} f(x) \bigg|_{x=T^{-1}(z)}$$
$$\dot{\xi} = A_c \xi + B_c[\alpha(x) + \mathcal{B}(x)u]$$
$$y = C_c \xi \tag{8}$$

where $A_c = \text{diag}\{A_0^i\}$, $B_c = \text{diag}\{B_0^i\}$, $C_c = \text{diag}\{C_0^i\}$, $i = 1, 2, \ldots, m$, and (A_0^i, B_0^i, C_0^i) is a canonical form representation of a chain of ρ_i integrators.

Assume $\mathcal{B}(x)$ is nonsingular; otherwise, $p = m$ would still lead to an underdetermined problem. The nonlinear dynamic inversion (NDI) linearization is designed as $u = \mathcal{B}^{-1}(x)(\nu - \alpha(x))$, where $\nu \in \mathbb{R}^m$ is called the pseudocontrol input. In the absence of model uncertainties and disturbances, this linearization results in the closed-loop system

$$\dot{\eta} = f_0(\eta, \xi)$$
$$\dot{\xi} = A_c \xi + B_c \nu$$
$$y = C_c \xi \tag{9}$$

which indicates that this closed-loop system has $n - \rho$ internal dynamics and m decoupled channels. The input–output mapping for each channel from ν_i to y_i is a chain of ρ_i integrators.

NDI linearization, however, is based on the exact mathematical cancellation of the nonlinear terms $\alpha(x)$ and $\mathcal{B}(x)$. This is almost

impossible in practice due to model simplifications, computational errors, and external disturbances. One method to reduce the control law model dependency is incremental nonlinear dynamic inversion (INDI), which will be reformulated here. Take the first-order Taylor series expansion of Eq. (5) around the condition at $t - \Delta t$ (denoted by the subscript 0) as

$$
\begin{aligned}
\boldsymbol{y}^{(\rho)} &= \boldsymbol{\alpha}(\boldsymbol{x}) + \boldsymbol{\mathcal{B}}(\boldsymbol{x})\boldsymbol{u} \\
&= \boldsymbol{y}_0^{(\rho)} + \frac{\partial[\boldsymbol{\alpha}(\boldsymbol{x}) + \boldsymbol{\mathcal{B}}(\boldsymbol{x})\boldsymbol{u}]}{\partial \boldsymbol{x}}\bigg|_0 \Delta\boldsymbol{x} + \boldsymbol{\mathcal{B}}(\boldsymbol{x}_0)\Delta\boldsymbol{u} + \mathcal{O}(\Delta\boldsymbol{x}^2) \\
&= \boldsymbol{y}_0^{(\rho)} + \boldsymbol{\mathcal{B}}(\boldsymbol{x}_0)\Delta\boldsymbol{u} + \boldsymbol{\delta}(\boldsymbol{z}, \Delta t)
\end{aligned}
\tag{10}
$$

where $\Delta\boldsymbol{x}$ and $\Delta\boldsymbol{u}$ represent the state and control increments in one sampling time step Δt. $\boldsymbol{\delta}(\boldsymbol{z}, \Delta t)$ is given by

$$
\boldsymbol{\delta}(\boldsymbol{z}, \Delta t) = \left[\frac{\partial[\boldsymbol{\alpha}(\boldsymbol{x}) + \boldsymbol{\mathcal{B}}(\boldsymbol{x})\boldsymbol{u}]}{\partial \boldsymbol{x}}\bigg|_0 \Delta\boldsymbol{x} + \mathcal{O}(\Delta\boldsymbol{x}^2)\right]\bigg|_{\boldsymbol{x}=\boldsymbol{T}^{-1}(\boldsymbol{z})}
\tag{11}
$$

Design the incremental control input as

$$
\Delta\boldsymbol{u} = \boldsymbol{\mathcal{B}}^{-1}(\boldsymbol{x}_0)(\boldsymbol{\nu} - \boldsymbol{y}_0^{(\rho)})
\tag{12}
$$

where $\boldsymbol{y}_0^{(\rho)}$ is measured or estimated. The total control command for the actuator is $\boldsymbol{u} = \boldsymbol{u}_0 + \Delta\boldsymbol{u}$. Substituting Eq. (12) into Eq. (10) results in the input–output mapping of $\boldsymbol{y}^{(\rho)} = \boldsymbol{\nu} + \boldsymbol{\delta}(\boldsymbol{z}, \Delta t)$. Using the same diffeomorphism $\boldsymbol{z} = \boldsymbol{T}(\boldsymbol{x})$, the closed-loop system dynamics under INDI linearization are given by

$$
\begin{aligned}
\dot{\boldsymbol{\eta}} &= \boldsymbol{f}_0(\boldsymbol{\eta}, \boldsymbol{\xi}) \\
\dot{\boldsymbol{\xi}} &= \boldsymbol{A}_c\boldsymbol{\xi} + \boldsymbol{B}_c[\boldsymbol{\nu} + \boldsymbol{\delta}(\boldsymbol{z}, \Delta t)] \\
\boldsymbol{y} &= \boldsymbol{C}_c\boldsymbol{\xi}
\end{aligned}
\tag{13}
$$

which is consistent with Eq. (9), except for the perturbation term $\boldsymbol{\delta}(\boldsymbol{z}, \Delta t)$. Because $\boldsymbol{x}$ is continuously differentiable, the norm value of $\boldsymbol{\delta}(\boldsymbol{z}, \Delta t)$ can be reduced by increasing the sampling frequency. The influence of $\boldsymbol{\delta}(\boldsymbol{z}, \Delta t)$ on system stability and robustness will be elaborated in Sec. III. Although Eq. (9) under NDI control seems to be neat, perturbation terms will appear when model uncertainties and external disturbances are considered, which will also be shown in Sec. III. As compared to the conventional NDI control law, the INDI control method is less sensitive to model mismatches because $\boldsymbol{\alpha}(\boldsymbol{x})$ is not used in Eq. (12). On the other hand, this INDI control law needs the measurement or estimation of $\boldsymbol{y}_0^{(\rho)}$ and the actuator position $\boldsymbol{u}_0$; this is why INDI control is referred to as a sensor-based approach.

B. Output Tracking

INDI control can also be designed for the command tracking problem. Consider the nonlinear plant [Eq. (1)] with relative degree $\boldsymbol{\rho} = [\rho_1, \rho_2, \ldots, \rho_m]^T$, which can be transformed into the internal and external dynamics given by Eq. (8). The output tracking problem requires the output $\boldsymbol{y}$ to asymptotically track a reference signal $\boldsymbol{r}(t) = [r_1(t), r_2(t), \ldots, r_m(t)]^T$. Assume that $r_i(t), i = 1, 2, \ldots, m$ and its derivatives up to $r_i^{(\rho_i)}(t)$ are bounded for all t, and $r_i^{(\rho_i)}(t)$ is piecewise continuous. Denote the reference and the tracking error vectors as

$$
\begin{aligned}
\boldsymbol{\mathcal{R}} &= [\boldsymbol{\mathcal{R}}_1; \boldsymbol{\mathcal{R}}_2; \ldots; \boldsymbol{\mathcal{R}}_m], \quad \boldsymbol{\mathcal{R}}_i = \left[r_i, r_i^{(1)}, \ldots, r_i^{(\rho_i-1)}\right]^T, \\
&\quad i = 1, 2, \ldots, m, \quad \boldsymbol{e} = \boldsymbol{\xi} - \boldsymbol{\mathcal{R}}
\end{aligned}
\tag{14}
$$

Using the definitions of the $\boldsymbol{A}_c$ and $\boldsymbol{B}_c$ matrices and the formulation of $\boldsymbol{\mathcal{R}}$, it can be derived that $\boldsymbol{A}_c\boldsymbol{\mathcal{R}} - \dot{\boldsymbol{\mathcal{R}}} = -\boldsymbol{B}_c\boldsymbol{r}^{(\rho)}$, with $\boldsymbol{r}^{(\rho)} = [r_1^{(\rho_1)}, r_2^{(\rho_2)}, \ldots, r_m^{(\rho_m)}]^T$. Therefore, Eq. (8) can be transformed into

$$
\begin{aligned}
\dot{\boldsymbol{\eta}} &= \boldsymbol{f}_0(\boldsymbol{\eta}, \boldsymbol{e} + \boldsymbol{\mathcal{R}}) \\
\dot{\boldsymbol{e}} &= \boldsymbol{A}_c\boldsymbol{e} + \boldsymbol{A}_c\boldsymbol{\mathcal{R}} - \dot{\boldsymbol{\mathcal{R}}} + \boldsymbol{B}_c[\boldsymbol{\alpha}(\boldsymbol{x}) + \boldsymbol{\mathcal{B}}(\boldsymbol{x})\boldsymbol{u}] \\
&= \boldsymbol{A}_c\boldsymbol{e} + \boldsymbol{B}_c\left[\boldsymbol{\alpha}(\boldsymbol{x}) + \boldsymbol{\mathcal{B}}(\boldsymbol{x})\boldsymbol{u} - \boldsymbol{r}^{(\rho)}\right]
\end{aligned}
\tag{15}
$$

The NDI control for output tracking is designed as

$$
\boldsymbol{u} = \boldsymbol{\mathcal{B}}^{-1}(\boldsymbol{x})\left[\boldsymbol{\nu} - \boldsymbol{\alpha}(\boldsymbol{x}) + \boldsymbol{r}^{(\rho)}\right]
\tag{16}
$$

When perfect model cancellation is assumed, this NDI control law results in the closed-loop system

$$
\dot{\boldsymbol{\eta}} = \boldsymbol{f}_0(\boldsymbol{\eta}, \boldsymbol{e} + \boldsymbol{\mathcal{R}}), \quad \dot{\boldsymbol{e}} = \boldsymbol{A}_c\boldsymbol{e} + \boldsymbol{B}_c\boldsymbol{\nu}
\tag{17}
$$

On the other hand, by using Eq. (10), the INDI control for output tracking is designed as

$$
\Delta\boldsymbol{u} = \boldsymbol{\mathcal{B}}^{-1}(\boldsymbol{x}_0)\left[\boldsymbol{\nu} - \boldsymbol{y}_0^{(\rho)} + \boldsymbol{r}^{(\rho)}\right]
\tag{18}
$$

which leads to the closed-loop system as

$$
\dot{\boldsymbol{\eta}} = \boldsymbol{f}_0(\boldsymbol{\eta}, \boldsymbol{e} + \boldsymbol{\mathcal{R}}), \quad \dot{\boldsymbol{e}} = \boldsymbol{A}_c\boldsymbol{e} + \boldsymbol{B}_c[\boldsymbol{\nu} + \boldsymbol{\delta}(\boldsymbol{z}, \Delta t)]
\tag{19}
$$

The closed-loop system dynamics given by Eqs. (13) and (19) are essentially the same. Only the equilibrium point of $\boldsymbol{z} = [\boldsymbol{\eta}; \boldsymbol{\xi}] = \boldsymbol{0}$ is shifted to $\boldsymbol{z}' = [\boldsymbol{\eta}; \boldsymbol{e}] = \boldsymbol{0}$, and so similar stability and robustness analyses can be made.

C. Input-to-State Linearization Under Disturbance Perturbations

Consider a special case of input–output linearization by taking the outputs as $y_i = h_i(\boldsymbol{x}) = x_i - x_{i*}, \; i = 1, 2, \ldots, m$, or equally $\boldsymbol{y} = \boldsymbol{H}(\boldsymbol{x} - \boldsymbol{x}_*)$, where $\boldsymbol{H}$ is a Boolean selection matrix, and $\boldsymbol{x}_*$ is the equilibrium point. This choice of output results in a so-called symmetrical system [24], where all m channels have the same relative degree $\rho_i = 1$, and the total relative degree is $\rho = m$. When $m < n$, there are $n - m$ internal dynamics.

Adding the disturbance perturbation $\boldsymbol{d} \in \mathbb{R}^n$ into the nonlinear plant [Eq. (1)] as

$$
\begin{aligned}
\dot{\boldsymbol{x}} &= \boldsymbol{f}(\boldsymbol{x}) + \boldsymbol{G}(\boldsymbol{x})\boldsymbol{u} + \boldsymbol{d} \\
\boldsymbol{y} &= \boldsymbol{H}(\boldsymbol{x} - \boldsymbol{x}_*)
\end{aligned}
\tag{20}
$$

Recall Eq. (7); because $\rho_i = 1$, the external states are given by $\xi_i = h_i(\boldsymbol{x}) = x_i - x_{i*}, i = 1, 2, \ldots, m$, with dynamics

$$
\dot{\boldsymbol{y}} = \dot{\boldsymbol{\xi}} = \bar{\boldsymbol{f}}(\boldsymbol{\xi}) + \bar{\boldsymbol{G}}(\boldsymbol{\xi})\boldsymbol{u} + \boldsymbol{H}\boldsymbol{d}
\tag{21}
$$

where $\bar{\boldsymbol{f}}: \mathbb{R}^m \to \mathbb{R}^m$ and $\bar{\boldsymbol{G}}: \mathbb{R}^m \to \mathbb{R}^{m \times m}$ can be calculated by substituting $x_i = \xi_i + x_{i*}, \; i = 1, 2, \ldots, m$ into Eq. (20). Take the first-order Taylor series expansion of the external dynamic equations as

$$
\begin{aligned}
\dot{\boldsymbol{\xi}} &= \bar{\boldsymbol{f}}(\boldsymbol{\xi}) + \bar{\boldsymbol{G}}(\boldsymbol{\xi})\boldsymbol{u} + \boldsymbol{H}\boldsymbol{d} \\
&= \dot{\boldsymbol{\xi}}_0 + \frac{\partial[\bar{\boldsymbol{f}}(\boldsymbol{\xi}) + \bar{\boldsymbol{G}}(\boldsymbol{\xi})\boldsymbol{u}]}{\partial \boldsymbol{\xi}}\bigg|_0 \Delta\boldsymbol{\xi} + \bar{\boldsymbol{G}}(\boldsymbol{\xi}_0)\Delta\boldsymbol{u} + \boldsymbol{H}\Delta\boldsymbol{d} + \mathcal{O}(\Delta\boldsymbol{\xi}^2) \\
&= \dot{\boldsymbol{\xi}}_0 + \bar{\boldsymbol{G}}(\boldsymbol{\xi}_0)\Delta\boldsymbol{u} + \boldsymbol{H}\Delta\boldsymbol{d} + \boldsymbol{\delta}(\boldsymbol{\xi}, \Delta t)
\end{aligned}
\tag{22}
$$

In the preceding equation, the remainder term $\mathcal{O}$ is only a function of $\Delta\boldsymbol{\xi}^2$. This is because the higher-order partial derivatives $\partial^i\dot{\boldsymbol{\xi}}/\partial\boldsymbol{u}^i$ and $\partial^i\dot{\boldsymbol{\xi}}/\partial\boldsymbol{d}^i$ for $i \geq 2$ are all equal to zero. Design the incremental control law as $\Delta\boldsymbol{u} = \bar{\boldsymbol{G}}^{-1}(\boldsymbol{\xi}_0)(\boldsymbol{\nu} - \dot{\boldsymbol{\xi}}_0)$; the closed-loop external dynamics are formulated by

$$
\dot{\boldsymbol{\xi}} = \boldsymbol{\nu} + \boldsymbol{H}\Delta\boldsymbol{d} + \boldsymbol{\delta}(\boldsymbol{\xi}, \Delta t)
\tag{23}
$$

Analogously, using Eq. (6), the internal dynamics under disturbance perturbations are given by

$$\dot{\eta} = \frac{\partial \phi}{\partial x}(f(x) + G(x)u + d) = \frac{\partial \phi}{\partial x}(f(x) + d) = f_d(\eta, \xi, d) \tag{24}$$

where $f_d(\eta, \xi, d): \mathbb{R}^{n-\rho} \times \mathbb{R}^\rho \times \mathbb{R}^n \to \mathbb{R}^{n-\rho}$. Choosing $\phi(x_*) = \mathbf{0}$, the diffeomorphism $z = T(x) = [\eta; \xi]$ transforms the equilibrium $x = x_*$ into the origin point $z = [\eta; \xi] = \mathbf{0}$.

When $d = \mathbf{0}$, the input-to-state linearized closed-loop system dynamics given by Eqs. (23) and (24) are a special case of Eq. (13). It can also be observed from Eqs. (23) and (24) that the disturbance d influences the external dynamics only by its increments Δd, whereas it directly influences the internal dynamics. Most external disturbances in real life are continuous; thus, $\lim_{\Delta t \to 0} \|d\|_2 = 0$. In other words, when $d \neq \mathbf{0}$, $\exists \Delta t$, such that $\|\Delta d\|_2 < \|d\|_2$. This is another feature of INDI control, in which the main part of the disturbance influences have already been included by previous measurements and compensated by the controller. This control method thus presents improved disturbance rejection ability as verified by simulations [15,21] and flight tests [13,14]. This feature of INDI will be further analyzed in Sec. III.

III. Stability and Robustness Analysis

The stability and robustness of the reformulated INDI control will be analyzed in this section. In the first subsection, the influences of the state-variation-related terms on closed-loop system stability will be discussed. The second subsection discusses the system robustness to regular and singular perturbations.

A. Stability Analysis

In this subsection, the stability of the origin $z = \mathbf{0}$ of closed-loop system given by Eq. (13) under INDI control will be analyzed. Similar conclusions can be drawn for systems modeled by Eq. (19) and Eqs. (23) and (24) without disturbances. The closed-loop system under the perturbations of external disturbances and model uncertainties will be analyzed in Sec. III.B. The proofs in this section also assume ideal actuators and perfect sensing. The actuator dynamics, nonlinear limits of actuators, and the sensing issues will also be discussed in Sec. III.B.

Design the pseudocontrol $\nu = -K\xi$, such that $A_c - B_c K$ is Hurwitz; Eq. (13) results in

$$\dot{\eta} = f_0(\eta, \xi)$$
$$\dot{\xi} = (A_c - B_c K)\xi + B_c \delta(z, \Delta t) \tag{25}$$

where the output equation is dropped because it plays no role in the stabilization problem.

Remark: The term $\delta(z, \Delta t)$ in Eq. (10) or the term $\delta(\xi, \Delta t)$ in Eq. (22) is directly omitted in the literature [7,10–20] by claiming that the Δz (or $\Delta \xi$) related term is smaller than the Δu related term when the sampling frequency is high, which is referred to as the time scale separation principle (different from the widely used separation principle based on singular perturbation theory). This statement is not mathematically rigorous and is especially deficient for unstable nonlinear plants because the plant simplifications are made before designing the INDI control inputs. Consequently, the simplified (by omitting terms) incremental dynamic equations fail to adequately model the plant dynamics. Moreover, although these terms are dropped out for the convenience of controller design, they should be kept in the closed-loop system equations and remain influencing the stability and performance, which has been overlooked in the literature.

Consider the following system as the nominal system:

$$\dot{\eta} = f_0(\eta, \xi)$$
$$\dot{\xi} = (A_c - B_c K)\xi \tag{26}$$

whose stability has been extensively proved in the literature and is listed here for completeness.

Lemma 1: The origin of Eq. (26) is asymptotically stable if the origin of $\dot{\eta} = f_0(\eta, \mathbf{0})$ is asymptotically stable.

$\dot{\eta} = f_0(\eta, \mathbf{0})$ is referred to as the zero dynamics, and the nonlinear system is said to be minimum phase if its zero dynamics has an asymptotically stable equilibrium point.

Lemma 2: The origin of Eq. (26) is globally asymptotically stable if the system $\dot{\eta} = f_0(\eta, \xi)$ is input-to-state stable.

The proofs for Lemma 1 and Lemma 2 can be found in [2]. After presenting stability of the nominal system, the stability of the perturbed system given by Eq. (25) will be considered. Recall Eq. (11); the norm value of the perturbation term is

$$\|\delta(x, \Delta t)\|_2 = \|\delta(z, \Delta t)|_{z=T(x)}\|_2$$
$$= \left\| \frac{\partial[\alpha(x) + \mathcal{B}(x)u]}{\partial x} \bigg|_0 \Delta x + \mathcal{O}(\Delta x^2) \right\|_2 \tag{27}$$

Assume the partial derivatives of $\alpha(x)$ and $\mathcal{B}(x)$ with respect to x up to any order are bounded. Because of the continuity of x,

$$\lim_{\Delta t \to 0} \|\Delta x\|_2 = 0$$

Therefore, the perturbation term satisfies

$$\lim_{\Delta t \to 0} \|\delta(z, \Delta t)\|_2 = 0, \quad \forall z \in \mathbb{R}^n \tag{28}$$

which means that the norm value of this perturbation term becomes negligible for sufficiently high sampling frequency. Equation (28) also indicates that $\forall \bar{\delta}_\varepsilon > 0, \exists \overline{\Delta t} > 0$, such that for all $0 < \Delta t \le \overline{\Delta t}$, $\forall z \in \mathbb{R}^n, \forall t \ge t_0, \|\delta(z, \Delta t)\|_2 \le \bar{\delta}_\varepsilon$. In other words, there exists a Δt that guarantees the boundedness of $\delta(z, \Delta t)$. Also, this bound can be further diminished by increasing the sampling frequency.

Theorem 1: If $\|\delta(z, \Delta t)\|_2 \le \bar{\delta}_\varepsilon$ is satisfied for all $z \in \mathbb{R}^n$, and $\dot{\eta} = f_0(\eta, \xi)$ is input-to-state stable, then the state z of Eq. (25) is globally ultimately bounded by a class $\mathcal{K}$ function of $\bar{\delta}_\varepsilon$.

Proof: Choose the candidate Lyapunov function as $V(\xi) = \xi^T P \xi$, where $P = P^T > 0$ is the solution of the Lyapunov equation $P(A_c - B_c K) + (A_c - B_c K)^T P = -I$; then, $V(\xi)$ is positive-definite and satisfies

$$\alpha_1(\|\xi\|_2) \le V(\xi) \le \alpha_2(\|\xi\|_2)$$
$$\alpha_1(\|\xi\|_2) \triangleq \lambda_{\min}(P)\|\xi\|_2^2, \quad \alpha_2(\|\xi\|_2) \triangleq \lambda_{\max}(P)\|\xi\|_2^2 \tag{29}$$

$\lambda_{\min}(P), \lambda_{\max}(P)$ are the minimum and maximum eigenvalues of the P matrix. α_1, α_2 belong to the class $\mathcal{K}_\infty$ functions. The time derivative of the candidate Lyapunov function is calculated as

$$\dot{V} = \xi^T[P(A_c - B_c K) + (A_c - B_c K)^T P]\xi + 2\xi^T P B_c \delta(z, \Delta t)$$
$$\le -\|\xi\|_2^2 + 2\|\xi\|_2\|P B_c\|_2 \bar{\delta}_\varepsilon$$
$$\le -\theta_1\|\xi\|_2^2, \quad \forall \|\xi\|_2 \ge \frac{2\|P B_c\|_2 \bar{\delta}_\varepsilon}{1 - \theta_1} \triangleq \mu_1 \bar{\delta}_\varepsilon \tag{30}$$

with constant $\theta_1 \in (0, 1)$. Consequently, for $\forall \xi(t_0) \in \mathbb{R}^\rho$, there exists a class $\mathcal{KL}$ function β and finite $T_1 \ge 0$ independent of t_0 such that $\|\xi(t)\|_2$ satisfies [2]

$$\|\xi(t)\|_2 \le \beta(\|\xi(t_0)\|_2, t - t_0), \quad t_0 \le \forall t \le t_0 + T_1$$
$$\|\xi(t)\|_2 \le \alpha_1^{-1}(\alpha_2(\mu_1 \bar{\delta}_\varepsilon)), \quad \forall t \ge t_0 + T_1 \triangleq t_0' \tag{31}$$

The preceding equations indicate that the external state ξ is bounded for all $t \ge t_0$ and is ultimately bounded by $\Gamma \bar{\delta}_\varepsilon \triangleq \alpha_1^{-1}(\alpha_2(\mu_1 \bar{\delta}_\varepsilon)) = \sqrt{\lambda_{\max}(P)/\lambda_{\min}(P)}\mu_1 \bar{\delta}_\varepsilon$.

Moreover, by the definition of input-to-state stability, there exists a class $\mathcal{KL}$ function β_0 and a class $\mathcal{K}$ function γ_0 such that, for $\forall \eta(t_0') \in \mathbb{R}^{n-\rho}$ and bounded input ξ, the internal state η satisfies

$$\|\boldsymbol{\eta}(t)\|_2 \leq \beta_0\Big(\|\boldsymbol{\eta}(t_0')\|_2, t - t_0'\Big) + \gamma_0\Big(\sup_{t_0' \leq \tau \leq t} \|\boldsymbol{\xi}(\tau)\|_2\Big)$$

$$= \beta_0\Big(\|\boldsymbol{\eta}(t_0')\|_2, t - t_0'\Big) + \gamma_0(\Gamma\bar{\delta}_\varepsilon) \tag{32}$$

In addition, because β_0 belongs to class $\mathcal{KL}$ functions, $\beta_0(\|\boldsymbol{\eta}(t_0')\|_2, t - t_0') \leq \theta_2\bar{\delta}_\varepsilon$, for some finite $T_2 > 0$ and $\theta_2 > 0$. Hence, the state z satisfies

$$\|\boldsymbol{z}(t)\|_2 \leq \|\boldsymbol{\xi}(t)\|_2 + \|\boldsymbol{\eta}(t)\|_2 = (\Gamma + \theta_2)\bar{\delta}_\varepsilon + \gamma_0(\Gamma\bar{\delta}_\varepsilon),$$

$$\forall\, t \geq t_0 + T_1 + T_2 \tag{33}$$

which proves that $\boldsymbol{z}(t)$ is globally ultimately bounded by a class $\mathcal{K}$ function of $\bar{\delta}_\varepsilon$. This completes the proof. $\square$

Theorem 1 has no restriction on the values of the initial state and the perturbation bound $\bar{\delta}_\varepsilon$. However, when the internal dynamics $\dot{\boldsymbol{\eta}} = \boldsymbol{f}_0(\boldsymbol{\eta}, \boldsymbol{\xi})$ is not input-to-state stable, but only the origin of the zero dynamics $\dot{\boldsymbol{\eta}} = \boldsymbol{f}_0(\boldsymbol{\eta}, \boldsymbol{0})$ is exponentially stable, then there will be restrictions on both the initial state and the perturbations. These phenomena are presented in Theorem 2.

Theorem 2: If $\|\boldsymbol{\delta}(\boldsymbol{z}, \Delta t)\|_2 \leq \bar{\delta}_\varepsilon$ is satisfied for all $\boldsymbol{z} \in \mathbb{R}^n$, and the origin of $\dot{\boldsymbol{\eta}} = \boldsymbol{f}_0(\boldsymbol{\eta}, \boldsymbol{0})$ is exponentially stable, then there is a neighborhood D_z of $\boldsymbol{z} = \boldsymbol{0}$ and $\varepsilon^* > 0$, such that, for every $\boldsymbol{z}(0) \in D_z$ and $\bar{\delta}_\varepsilon < \varepsilon^*$, the state $\boldsymbol{z}$ of Eq. (25) is ultimately bounded by a class $\mathcal{K}$ function of $\bar{\delta}_\varepsilon$.

Proof: According to the converse Lyapunov theorem [2], because the origin of $\dot{\boldsymbol{\eta}} = \boldsymbol{f}_0(\boldsymbol{\eta}, \boldsymbol{0})$ is exponentially stable, there exists a Lyapunov function $V_2(\boldsymbol{\eta})$ defined in $D_\eta = \{\boldsymbol{\eta} \in \mathbb{R}^{n-\rho} | \|\boldsymbol{\eta}\| < r_\eta\}$ that satisfies the inequalities

$$c_1\|\boldsymbol{\eta}\|_2^2 \leq V_2(\boldsymbol{\eta}) \leq c_2\|\boldsymbol{\eta}\|_2^2, \quad \frac{\partial V_2}{\partial \boldsymbol{\eta}} \boldsymbol{f}_0(\boldsymbol{\eta}, \boldsymbol{0}) \leq -c_3\|\boldsymbol{\eta}\|_2^2,$$

$$\left\|\frac{\partial V_2}{\partial \boldsymbol{\eta}}\right\|_2 \leq c_4\|\boldsymbol{\eta}\|_2 \tag{34}$$

for some positive constants c_1, c_2, c_3, c_4. Denote

$$\alpha_1'(\|\boldsymbol{\eta}\|_2) \triangleq c_1\|\boldsymbol{\eta}\|_2^2, \quad \alpha_2'(\|\boldsymbol{\eta}\|_2) \triangleq c_2\|\boldsymbol{\eta}\|_2^2 \tag{35}$$

then α_1', α_2' belong to class $\mathcal{K}_\infty$ functions. Furthermore, because $\boldsymbol{f}_0$ is continuous and differentiable, there exists a Lipschitz constant L of $\boldsymbol{f}_0$ with respect to $\boldsymbol{\xi}$ such that

$$\|\boldsymbol{f}_0(\boldsymbol{\eta}, \boldsymbol{\xi}) - \boldsymbol{f}_0(\boldsymbol{\eta}, \boldsymbol{0})\|_2 \leq L\|\boldsymbol{\xi}\|_2, \quad \forall\, \|\boldsymbol{\eta}\| < r_\eta \tag{36}$$

Choose $V_2(\boldsymbol{\eta})$ as the candidate Lyapunov function for $\dot{\boldsymbol{\eta}} = \boldsymbol{f}_0(\boldsymbol{\eta}, \boldsymbol{\xi})$, with derivative

$$\dot{V}_2(\boldsymbol{\eta}) = \frac{\partial V_2}{\partial \boldsymbol{\eta}} \boldsymbol{f}_0(\boldsymbol{\eta}, \boldsymbol{0}) + \frac{\partial V_2}{\partial \boldsymbol{\eta}} [\boldsymbol{f}_0(\boldsymbol{\eta}, \boldsymbol{\xi}) - \boldsymbol{f}_0(\boldsymbol{\eta}, \boldsymbol{0})]$$

$$\leq -c_3\|\boldsymbol{\eta}\|_2^2 + c_4L\|\boldsymbol{\eta}\|_2\|\boldsymbol{\xi}\|_2$$

$$\leq -c_3(1 - \theta_3)\|\boldsymbol{\eta}\|_2^2, \quad \frac{c_4L\|\boldsymbol{\xi}\|_2}{c_3\theta_3} \leq \forall\, \|\boldsymbol{\eta}\|_2 \leq r_\eta \tag{37}$$

with constant $\theta_3 \in (0, 1)$. Denote

$$\mu \triangleq \frac{c_4L}{c_3\theta_3}\Big(\sup_{t_0' \leq \tau \leq t} \|\boldsymbol{\xi}(\tau)\|_2\Big) \triangleq \theta_5\Big(\sup_{t_0' \leq \tau \leq t} \|\boldsymbol{\xi}(\tau)\|_2\Big) \tag{38}$$

then

$$\dot{V}_2(\boldsymbol{\eta}) \leq -c_3(1 - \theta_3)\|\boldsymbol{\eta}\|_2^2, \quad \mu \leq \forall\, \|\boldsymbol{\eta}\|_2 \leq r_\eta, \quad \forall\, t \geq t_0' \tag{39}$$

Because the conditions for the external states $\boldsymbol{\xi}$ are the same as compared to Theorem 1, Eqs. (29), (30), and (31) also hold true in this

theorem. From Eq. (31), the supremum of the external state is given by

$$\sup_{t_0' \leq \tau \leq t} \|\boldsymbol{\xi}(\tau)\|_2 = \alpha_1^{-1}\Big(\alpha_2(\mu_1\bar{\delta}_\varepsilon)\Big) \tag{40}$$

Take $0 < r < r_\eta$ such that $D_r \subset D_\eta$; according to the boundedness theories [2], if

$$\mu < \alpha_2'^{-1}(\alpha_1'(r)), \quad \|\boldsymbol{\eta}(t_0')\|_2 \leq \alpha_2'^{-1}(\alpha_1'(r)) \tag{41}$$

then there exists a class $\mathcal{KL}$ function β_0' such that

$$\|\boldsymbol{\eta}(t)\|_2 \leq \beta_0'\Big(\|\boldsymbol{\eta}(t_0')\|_2, t - t_0'\Big) + \alpha_1'^{-1}(\alpha_2'(\mu)), \quad \forall\, t \geq t_0' \tag{42}$$

Equation (41) proposes requirements on both the initial condition and the perturbation bound. Using Eqs. (38), (40), and (41), the maximum perturbation that the system can sustain is given by

$$\bar{\delta}_\varepsilon < \varepsilon^* \triangleq (1/\mu_1)\alpha_2^{-1}\Big(\alpha_1\Big((1/\theta_5)\alpha_2'^{-1}(\alpha_1'(r))\Big)\Big) \tag{43}$$

From Eqs. (38), (40), and (42), the normal value of the internal state yields

$$\|\boldsymbol{\eta}(t)\|_2 \leq \beta_0'\Big(\|\boldsymbol{\eta}(t_0')\|_2, t - t_0'\Big) + \alpha_1'^{-1}\Big(\alpha_2'\Big(\theta_5\alpha_1^{-1}(\alpha_2(\mu_1\bar{\delta}_\varepsilon))\Big)\Big)$$

$$\leq \theta_6\bar{\delta}_\varepsilon + \theta_5\alpha_1'^{-1}\Big(\alpha_2'\Big(\alpha_1^{-1}(\alpha_2(\mu_1\bar{\delta}_\varepsilon))\Big)\Big), \quad \forall t \geq t_0 + T_1 + T_3 \tag{44}$$

for some finite $T_3 > 0$ and $\theta_6 > 0$. Hence, state z satisfies

$$\|\boldsymbol{z}(t)\|_2 \leq \|\boldsymbol{\xi}(t)\|_2 + \|\boldsymbol{\eta}(t)\|_2$$

$$= (\Gamma + \theta_6)\bar{\delta}_\varepsilon + \theta_5\alpha_1'^{-1}\Big(\alpha_2'\Big(\alpha_1^{-1}(\alpha_2(\mu_1\bar{\delta}_\varepsilon))\Big)\Big), \quad \forall t \geq t_0 + T_1 + T_3 \tag{45}$$

which proves that $\boldsymbol{z}(t)$ is ultimately bounded by a class $\mathcal{K}$ function of $\bar{\delta}_\varepsilon$. This completes the proof. $\square$

B. Robustness Analysis

1. Disturbance Rejection

The INDI control method has promising disturbance rejection ability, as has been verified by both simulations [15,21] and quadrotor flight tests [13,14]. However, there is a lack of theoretical proof for the stability of the closed-loop system using INDI control under the perturbation of external disturbances. These issues will be discussed in this subsection.

Normally, the external disturbances are bounded in real life. Denote

$$\bar{d} \triangleq \sup\{\|\boldsymbol{d}(t)\|_2, \boldsymbol{d} \in \mathbb{R}^n\}, \quad \forall\, t \geq t_0 \tag{46}$$

which is independent of the sampling interval Δt. Most external disturbances in real life are continuous; thus, $\lim_{\Delta t \to 0} \|\Delta \boldsymbol{d}\|_2 = 0$. Therefore, for a given sampling rate, the supremum of $\|\Delta \boldsymbol{d}\|_2$ exists. Denote

$$\bar{d}_\varepsilon(\Delta t) \triangleq \sup\{\|\Delta \boldsymbol{d}(t)\|_2, \Delta \boldsymbol{d} \in \mathbb{R}^n\}, \quad \forall\, t \geq t_0 \tag{47}$$

As a function of Δt, $\bar{d}_\varepsilon(\Delta t)$ can be reduced by increasing the sampling frequency. Recall the system modeled by Eqs. (23) and (24), and design the pseudocontrol as $\boldsymbol{\nu} = -\boldsymbol{K}\boldsymbol{\xi}$ to stabilize the origin $\boldsymbol{z} = [\boldsymbol{\eta}; \boldsymbol{\xi}] = \boldsymbol{0}$. The closed-loop system is then given by

$$\dot{\eta} = f_d(\eta, \xi, d)$$
$$\dot{\xi} = -K\xi + H\Delta d + \delta(\xi, \Delta t) \qquad (48)$$

Proposition 1: If $\|\delta(\xi, \Delta t)\|_2 \leq \bar{\delta}_\varepsilon$ is satisfied for all $\xi \in \mathbb{R}^\rho$, $\dot{\eta} = f_d(\eta, \xi, d)$ is continuously differentiable and globally Lipschitz in (η, ξ, d), and the origin of $\dot{\eta} = f_d(\eta, 0, 0)$ is globally exponentially stable, then the external state ξ is globally ultimately bounded by a class $\mathcal{K}$ function of $\bar{\delta}_\varepsilon, \bar{d}_\varepsilon$, whereas the internal state η of Eq. (48) is globally ultimately bounded by a class $\mathcal{K}$ function of $\bar{d}, \bar{\delta}_\varepsilon, \bar{d}_\varepsilon$.

Proof: The norm value of the perturbation term in Eq. (48) satisfies

$$\|H\Delta d + \delta(\xi, \Delta t)\|_2 \leq \|H\|_2 \|\Delta d\|_2 + \|\delta(\xi, \Delta t)\|_2 = \bar{d}_\varepsilon + \bar{\delta}_\varepsilon \qquad (49)$$

where $\|H\|_2 = 1$ because H is a Boolean selection matrix. Similar to the proof of Theorem 1, choose the candidate Lyapunov function as $V(\xi) = \xi^T P\xi$, where $P = P^T > 0$ is the solution of the Lyapunov equation $PK + K^T P = I$; then, the time derivative of $V(\xi)$ satisfies

$$\dot{V} \leq -\theta_1 \|\xi\|_2^2, \quad \forall \|\xi\|_2 \geq \frac{2\|P\|_2(\bar{\delta}_\varepsilon + \bar{d}_\varepsilon)}{1 - \theta_1} \triangleq \mu_2(\bar{\delta}_\varepsilon + \bar{d}_\varepsilon) \quad (50)$$

Therefore, $\forall \xi(t_0) \in \mathbb{R}^\rho$, there exists a class $\mathcal{KL}$ function β and $T_4 \geq 0$ independent of t_0 such that $\|\xi(t)\|_2$ satisfies

$$\|\xi(t)\|_2 \leq \beta\big(\|\xi(t_0)\|_2, t - t_0\big), \qquad t_0 \leq \forall t \leq t_0 + T_4$$
$$\|\xi(t)\|_2 \leq \alpha_1^{-1}\big(\alpha_2\big(\mu_2(\bar{\delta}_\varepsilon + \bar{d}_\varepsilon)\big)\big), \qquad \forall t \geq t_0 + T_4 \qquad (51)$$

In other words, the external state ξ is bounded for all $t \geq t_0$ and ultimately bounded by $\Gamma_\xi \triangleq \alpha_1^{-1}(\alpha_2(\mu_2(\bar{\delta}_\varepsilon + \bar{d}_\varepsilon)))$, which is a class $\mathcal{K}$ function of $\bar{\delta}_\varepsilon$ and $\bar{d}_\varepsilon$.

On the other hand, perturbations directly act on the internal dynamics. Because the origin of $\dot{\eta} = f_d(\eta, 0, 0)$ is globally exponentially stable, Eq. (34) is satisfied globally. Moreover, because $\dot{\eta} = f_d(\eta, \xi, d)$ is continuously differentiable and globally Lipschitz in (η, ξ, d), there exists a global Lipschitz constant L, such that

$$\|f_d(\eta, \xi, d) - f_d(\eta, 0, 0)\|_2 \leq L(\|\xi\|_2 + \|d\|_2), \quad \forall \eta \in \mathbb{R}^{n-\rho} \qquad (52)$$

Analogous to the proofs of Theorem 2, Eq. (39) is satisfied for $\forall \|\eta\|_2 \geq \mu'$ with $\mu' \triangleq \theta_5(\sup_{t_0+T_4 \leq \tau \leq t}(\|\xi(\tau)\|_2 + \|d(\tau)\|_2))$, and the internal state η satisfies

$$\|\eta(t)\|_2 \leq \beta_0'\big(\|\eta(t_0 + T_4)\|_2, t - t_0 - T_4\big) + \theta_5\alpha_1'^{-1}\big(\alpha_2'(\Gamma_\xi + \bar{d})\big),$$
$$\forall t \geq t_0 + T_4 \qquad (53)$$

without restrictions on the initial values and the bound of disturbances. Because of the attenuation property of β_0',

$$\|\eta(t)\|_2 \leq \left[\theta_7\bar{d} + \theta_5\alpha_1'^{-1}(\alpha_2'(\bar{d}))\right]$$
$$+ \theta_5\alpha_1'^{-1}\big(\alpha_2'\big(\alpha_1^{-1}\big(\alpha_2\big(\mu_2(\bar{\delta}_\varepsilon + \bar{d}_\varepsilon)\big)\big)\big)\big) \triangleq \Gamma_\eta, \quad \forall t \geq t_0 + T_4 + T_5 \qquad (54)$$

for some $\theta_7 > 0$ and finite $T_5 > 0$. The preceding equation indicates that η is globally ultimately bounded by a class $\mathcal{K}$ function of $\bar{d}, \bar{\delta}_\varepsilon, \bar{d}_\varepsilon$. This completes the proof. □

Remark: These estimations of the ultimate bounds could be conservative for a given perturbation term $H\Delta d + \delta(\xi, \Delta t)$ because the term $2\xi^T PB_c\delta(z, \Delta t)$ in Eq. (30) can be either positive or negative. Worst-case analyses are done in Eqs. (30) and (49) by taking the inequality constraints, which may lead to conservative estimations of the ultimate bounds. More accurate ultimate bounds of

a perturbed nonlinear system can be obtained via numerical simulations.

The disturbance rejection capability of a control method can be evaluated by the values of the ultimate bounds under prescribed disturbance perturbations. In view of Eqs. (51) and 54), the ultimate bounds Γ_ξ and Γ_η are correlated to the following:

1) System dynamics: Γ_ξ and Γ_η are functions of $\bar{\delta}_\varepsilon$. Recall Eq. (27); $\bar{\delta}_\varepsilon$ can be viewed as a gauge for system dynamics. When system dynamics are fast, which indicates that

$$\left\|\left.\frac{\partial[\alpha(x) + \mathcal{B}(x)u]}{\partial x}\right|_0\right\|_2$$

is large, the sampling frequency should be higher to ensure desired ultimate bounds. This has been verified by many application cases; for rigid airplane control, normally $f_s = 100$ Hz is enough [7,10,12,15,18–20], whereas $f_s = 1000$ Hz is needed for flexible aircraft control [21]. $f_s = 512$ Hz is used in Ref. [13,14] for quadrotor flight control. For the applications on hydraulic systems, $f_s = 5000$ Hz is desirable for controlling the hydraulic forces [16,17].

2) Disturbance intensity: this can be seen from the expressions for Γ_ξ, Γ_η and definitions of $\bar{d}, \bar{d}_\varepsilon$, in which stronger disturbances lead to larger ultimate bounds.

3) K gains: as shown in Eqs. (51) and (54), both Γ_ξ and Γ_η are monotonically increasing functions of μ_2. From Eq. (50) and the Lyapunov equation, it can be seen that larger K gains lead to smaller μ_2, further resulting in smaller ultimate bounds. Therefore, increasing K gains is beneficial for releasing the requirement on sampling frequency. However, K gains are constrained by actuation system limits; high-gain control would also amplify measurement noise.

4) Sampling frequency: recall Eqs. (28) and (47); both $\bar{d}_\varepsilon$ and $\bar{\delta}_\varepsilon$ can be reduced by increasing the sampling frequency. As discussed in Sec. II, if $d \neq 0$, $\|\Delta d\|_2 < \|d\|_2$ when the sampling interval Δt is sufficiently small. The main part of the disturbances d_0 can be included by the measurement of $\dot{\xi}_0$; thus, only the remaining increment Δd is perturbing ξ. This is one feature that distinguishes INDI from linear-quadratic regulator, proportional–integral, and NDI control methods, where normally the disturbances can only be reflected in the measurement of state ξ, which is an integration of $\dot{\xi}_0$. Consequently, these control methods show inferior disturbance rejection ability as compared to the INDI method. In practice, the choice of sampling frequency is constrained by the hardware.

5) Internal dynamics: it can be seen that the first term of Eq. (54) cannot be reduced by increasing the sampling frequency and is a function of $\bar{d}$. This is because the internal dynamics are uncontrolled by the INDI method. Moreover, being inspired by Theorem 2, when only the origin of $\dot{\eta} = f_d(\eta, 0, 0)$ is ensured to be exponentially stable or f_d is not globally Lipschitz, constraints on both initial condition and the disturbance intensity need to be imposed. This is presented as Corollary 1. Therefore, the properties of internal dynamics are important for the stability and robustness of the system.

Corollary 1: If $\|\delta(\xi, \Delta t)\|_2 \leq \bar{\delta}_\varepsilon$ is satisfied for all $\xi \in \mathbb{R}^\rho$, and the origin of $\dot{\eta} = f_0(\eta, 0, 0)$ is exponentially stable, then there is a neighborhood D_z of $z = 0$ and $\varepsilon^* > 0$, such that, for every $z(0) \in D_z$ and $(\bar{\delta}_\varepsilon + \bar{d}_\varepsilon) < \varepsilon^*$, the external state ξ in Eq. (48) is ultimately bounded by a class $\mathcal{K}$ function of $\bar{\delta}_\varepsilon, \bar{d}_\varepsilon$, whereas the internal state η in Eq. (48) is ultimately bounded by a class $\mathcal{K}$ function of $\bar{d}, \bar{\delta}_\varepsilon, \bar{d}_\varepsilon$.

The proof of Corollary 1 is similar to the proofs of Proposition 1 and Theorem 2.

2. Robustness to Model Uncertainties

The model uncertainties considered in this section are classified into the regular perturbations, which are defined in the nonlinear system perturbation theory as the perturbations that do not change the order of the nominal system, such as negligible nonlinearities, parametric dispersions, and variations [5,26].

There were few attempts at proving the robustness of the INDI control method to aerodynamics model uncertainties. In Ref. [10], it was shown by using linear transfer functions derived from block diagrams that the model mismatches of the control effectiveness

matrix $G(x)$ or the generalized $\mathcal{B}(x)$ has no influence on the closed-loop system. However, the assumption of $\dot{x} = \dot{x}_0$ is made in the block diagram derivations, which is incorrect because otherwise there will be no Δu term. Moreover, the $\delta(z, \Delta t)$ term did not show up at all in previous proofs [10,11,13]. In view of these reasons, the robustness of INDI to model uncertainties will be rediscussed here.

Considering the nonlinear system with relative degree $\rho \leq n$ transformed into internal and external dynamics given by Eqs. (7) and (8), the nominal NDI control to stabilize the system origin is given by

$$\bar{u}_{\text{ndi}} = \mathcal{B}^{-1}(x)(\nu - \alpha(x)) = \mathcal{B}^{-1}(x)(-KT_2(x) - \alpha(x)) \quad (55)$$

which requires the model knowledge of $\alpha, \mathcal{B}, T_2$ [defined in Eq. (7)]. When the control law is applied using the approximated model as $\hat{\alpha}, \hat{\mathcal{B}}, \hat{T}_2$, the control input is given as

$$u_{\text{ndi}} = \hat{\mathcal{B}}^{-1}(x)\left(-K\hat{T}_2(x) - \hat{\alpha}(x)\right) \quad (56)$$

which results in a closed-loop system as

$$\dot{\eta} = f_0(\eta, \xi)$$
$$\dot{\xi} = A_c\xi + B_c\left[\alpha(x) + \mathcal{B}(x)\hat{\mathcal{B}}^{-1}(x)\left(-K\hat{T}_2(x) - \hat{\alpha}(x)\right)\right]$$
$$= \left[A_c\xi - B_cK\hat{T}_2(x)\right] + B_c\left(\alpha(x) - \hat{\alpha}(x)\right)$$
$$+ B_c\left(\mathcal{B}(x)\hat{\mathcal{B}}^{-1}(x) - I\right)\left(-K\hat{T}_2(x) - \hat{\alpha}(x)\right)$$
$$= (A_c - B_cK)\xi + B_cK\left(T_2 - \hat{T}_2\right) + B_c(\alpha - \hat{\alpha})$$
$$+ B_c\left(\mathcal{B}\hat{\mathcal{B}}^{-1} - I\right)\left(-K\hat{T}_2 - \hat{\alpha}\right)$$
$$\triangleq (A_c - B_cK)\xi + B_c\varepsilon_{\text{ndi}}(z) \quad (57)$$

where $I \in \mathbb{R}^{m \times m}$ is an identity matrix. Using Eq. (12), the nominal INDI control for stabilization is given by

$$\Delta\bar{u}_{\text{indi}} = \mathcal{B}^{-1}(x_0)\left(-KT_2(x) - y_0^{(\rho)}\right) \quad (58)$$

When applied using estimated models, Eq. (58) becomes

$$\Delta u_{\text{indi}} = \hat{\mathcal{B}}^{-1}(x_0)\left(-K\hat{T}_2(x) - y_0^{(\rho)}\right) \quad (59)$$

and the closed-loop system dynamics are given by

$$\dot{\eta} = f_0(\eta, \xi)$$
$$\dot{\xi} = (A_c - B_cK)\xi + B_cK\left(T_2 - \hat{T}_2\right) + B_c\delta(z, \Delta t)$$
$$+ B_c\left(\mathcal{B}\hat{\mathcal{B}}^{-1} - I\right)\left(-K\hat{T}_2 - y_0^{(\rho)}\right)$$
$$\triangleq (A_c - B_cK)\xi + B_c\varepsilon_{\text{indi}}(z, \Delta t) \quad (60)$$

The regularly perturbed closed-loop dynamics given by Eqs. (57) and (60) are both in the form of Eq. (25). The only difference is the value of the perturbation terms. Therefore, it is straightforward to derive the corollaries of Theorem 1 and Theorem 2 as follows.

Corollary 2: If $\|\varepsilon_{\text{ndi/indi}}\|_2 \leq \bar{\varepsilon}_{\text{ndi/indi}}$ is satisfied for all $z \in \mathbb{R}^n$, and $\dot{\eta} = f_0(\eta, \xi)$ is input-to-state stable, then the states z of Eqs. (57) and (60) are globally ultimately bounded by a class $\mathcal{K}$ function of $\bar{\varepsilon}_{\text{ndi}}$ and $\bar{\varepsilon}_{\text{indi}}$, respectively.

Corollary 3: If $\|\varepsilon_{\text{ndi/indi}}\|_2 \leq \bar{\varepsilon}_{\text{ndi/indi}}$ is satisfied for all $z \in \mathbb{R}^n$, and the origin of $\dot{\eta} = f_0(\eta, 0)$ is exponentially stable, then there is a neighborhood D_z of $z = 0$ and $\varepsilon^* > 0$, such that for every $z(0) \in D_z$ and $\bar{\varepsilon}_{\text{ndi/indi}} < \varepsilon^*$, the states z of Eqs. (57) and (60) are ultimately bounded by a class $\mathcal{K}$ function of $\bar{\varepsilon}_{\text{ndi}}$ and $\bar{\varepsilon}_{\text{indi}}$, respectively.

Although the closed-loop dynamics given by Eqs. (57) and (60) have the same form, the perturbation terms $\varepsilon_{\text{ndi}}(z)$ and $\varepsilon_{\text{indi}}(z, \Delta t)$

have different properties, which consequently influence the ultimate bounds of the state z. This will be shown as follows.

The first perturbation term $K(T_2 - \hat{T}_2)$ is identical in ε_{ndi} [Eq. (57)] and $\varepsilon_{\text{indi}}$ [Eq. (60)]. For the second perturbation term, because INDI control Δu_{indi} is based on the measurements or estimations of $y_0^{(\rho)}$ instead of the dynamic model $\alpha(x)$, the model uncertainty term $\alpha(x) - \hat{\alpha}(x)$ in Eq. (57) is replaced by $\delta(z, \Delta t)$ [Eq. (60)] under INDI control. The influences of $\|\delta(z, \Delta t)\|_2$ become negligible when the sampling frequency is high, as indicated by Eq. (28), whereas $\|\alpha(x) - \hat{\alpha}(x)\|_2$ is normally large for aerospace systems, mainly because of the difficulties of modeling the aerodynamics. The last terms of $\varepsilon_{\text{ndi/indi}}$ are mainly caused by the multiplicative uncertainties of the $\mathcal{B}(x)$ matrix, which were incorrectly omitted in the previous literature [10,11,13,14]. Recall Eq. (59); the last term of $\varepsilon_{\text{indi}}$ can be written as

$$\left(\mathcal{B}\hat{\mathcal{B}}^{-1} - I\right)\left(-K\hat{T}_2 - y_0^{(\rho)}\right) = \left(\mathcal{B}\hat{\mathcal{B}}^{-1} - I\right)\hat{\mathcal{B}}\Delta u_{\text{indi}}$$
$$= \left(\mathcal{B} - \hat{\mathcal{B}}\right)\Delta u_{\text{indi}} \quad (61)$$

Because Δu_{indi} is a control increment, $\|\mathcal{B} - \hat{\mathcal{B}}^{-1}\|_2\|\Delta u_{\text{indi}}\|_2$ can be reduced by increasing the sampling rate. On the contrary, recall Eq. (56); the last term of ε_{ndi} equals

$$\left(\mathcal{B}\hat{\mathcal{B}}^{-1} - I\right)\left(-K\hat{T}_2 - \hat{\alpha}\right) = \left(\mathcal{B}\hat{\mathcal{B}}^{-1} - I\right)\hat{\mathcal{B}}u_{\text{ndi}} = \left(\mathcal{B} - \hat{\mathcal{B}}\right)u_{\text{ndi}} \quad (62)$$

which depends on the entire control term u_{ndi} and is independent of Δt. When $u_{\text{ndi}} \neq 0$, there exists a Δt such that $\|\Delta u_{\text{indi}}\|_2 < \|u_{\text{ndi}}\|_2$.

In summary, in the presence of model uncertainties, the norm of the closed-loop perturbation terms is smaller under INDI control and can be further diminished by increasing the sampling frequency. As a result, according to Corollary 2, when the internal dynamics $\dot{\eta} = f_0(\eta, \xi)$ are input-to-state stable, INDI control will result in smaller ultimate bounds for z. Moreover, when only the origin of $\dot{\eta} = f_0(\eta, 0)$ is exponentially stable, it is easier for systems under INDI control to fulfill the boundedness condition $\bar{\varepsilon}_{\text{ndi/indi}} < \varepsilon^*$ in Corollary 3.

3. Sensing and Singular Perturbations

Based on preceding analyses, INDI control has shown promising inherent robustness to disturbances and regular perturbations without using any additional robust or adaptive control technique. There are also other sources of perturbations, which increase the order of the system, such as actuator dynamics and higher-order elastic dynamics. These perturbations are classified into singular perturbations [5,26]. Consider the singularly perturbed system model as [2]

$$\dot{x} = f(t, x, z_p, \epsilon), \quad \epsilon\dot{z}_p = g_z(t, x, z_p, \epsilon) \quad (63)$$

where the perturbed dynamics are decomposed into reduced (slow) and boundary-layer (fast) dynamics. According to Tikhonov's theorem [2], when the null (quasi) equilibrium states of both the fast and slow dynamics are exponentially stable, there exists a constant $\epsilon_{\text{max}} > 0$ such that the null equilibrium of the singularly perturbed system is exponentially stable for all $\epsilon < \epsilon_{\text{max}}$. This parameter $\epsilon_{\text{max}} > 0$ is referred to as the singular perturbation margin in [26] and is equivalent to the phase margin of linear time-invariant systems in the sense of the bijective function [26].

Regarding the aerospace applications of INDI on angular rate control problems, the sensing or estimation of angular accelerations is needed [7,10–14,18–20]. Angular accelerometers are already available on the market [23], and a commonly used alternative way to estimate the angular accelerations is to differentiate the filtered angular rate signals [7,11–14,18–20]. Consequently, the estimations are lagged, owing to the filtering process. Smeur et al. [13,14], Huang et al. [17], and Grondman et al. [18] propose to synchronize the input signal with the lagged estimations by imposing the same filter on the

input. However, synchronization errors still exist in practice. Based on the preceding discussions, the system is able to sustain sufficiently small lags caused by filtering and actuator dynamics. This proposes an interesting research question of enlarging the singular perturbation margin of the closed-loop system. Possible solutions could be using predictive filters [10] or actuator compensators [27].

IV. Numerical Validation

Because there have been extensive applications of INDI on aircraft [10,15,18–20], helicopter [11], micro air vehicle [13], and spacecraft [12] angular velocity control, this problem will not be repeated here. The numerical example in this section considers a rigid aircraft gust load alleviation (GLA) problem, where the vertical velocity is included in the inner-loop INDI controller. This idea originates from [15], but the old INDI derivation in [15] also has the blemishes mentioned before. Therefore, this GLA problem will be resolved here using the reformulated INDI control. Section IV.A presents the aircraft and turbulence models. The INDI flight control is designed in Sec. IV.B. A command tracking problem in a turbulence field is considered in Sec. IV.C. The robustness of INDI to model uncertainties and external disturbances will be compared with NDI control in Sec. IV.D.

A. Aircraft and Turbulence Models

The six-degree-of-freedom rigid aircraft dynamic equations defined in the body frame are given by

$$\dot{V}_f = -\omega \times V_f + \frac{F}{m}, \quad \dot{\omega} = -J^{-1}\omega \times J\omega + J^{-1}M \quad (64)$$

where $V_f = [V_x, V_y, V_z]^T$ indicates the velocity of the aircraft c.m. relative to the inertial axis expressed in the body axis, and $\omega = [p, q, r]^T$ represents the angular velocity. m is the total mass, and J is the inertia matrix. F and M are the total forces and moments, which can be expanded as

$$F = F_a(V_f, \omega, V_w) + F_T(V_f, \delta_p) + F_{a_u}(V_f, \omega)u + F_G$$
$$M = M_a(V_f, \omega, V_w) + M_{a_u}(V_f, \omega)u \quad (65)$$

In the preceding equation, $u = [\delta_e, \delta_r, \delta_{ar}, \delta_{al}]^T$ denotes the elevator, rudder, and right and left aileron deflection angles. F_a and M_a denote the aerodynamic forces and moments when $u = 0$. V_w is the wind velocity. $F_{a_u}u$ and $M_{a_u}u$ represent the control forces and moments generated by the aerodynamic control surfaces. F_T is the thrust, as a function of throttle δ_p. F_G is the gravitational force.

The aircraft model for simulations is set up using the aerodynamic, inertia, and geometric data in [28]. The aerodynamic model is based on the quasi-steady strip theory [28,29]. This aircraft is abstracted to multiple two-dimensional aerodynamic surfaces. There are four aerodynamic control surfaces; each of them contains n_p strips. There are also six aerodynamic surfaces, namely the wing, horizontal and vertical tails, horizontal and vertical lifting surfaces of the fore fuselage, and the engine pylon. Each of these aerodynamic surfaces contains n_k strips. r_i denotes the distance vector from the c.m. to the aerodynamic center of the ith strip. The local airspeed of the ith strip

expressed in the body frame is $V_{a,i} = V_f + \omega \times r_i - V_{w,i}$, where $V_{w,i}$ is the local wind velocity [30,31]. In this paper, $V_{w,i}$ is calculated in real time by interpolating the spatial turbulence field at the aerodynamic center of the ith strip and then transformed to the body frame. The gust penetration effect [15,30,31] is considered because $V_{w,i}$ depends on the spatial location of the ith strip. A two-dimensional vertical von Kármán turbulence field is presented in Fig. 1, in which X_E and Y_E represent the positions in the inertial frame. The turbulence velocity is in unit meters per second. The turbulence length scale equals $L_g = 762$ m, and the variance equals $\sigma = 3$ m/s. Figure 1 also shows a sketch map of the aircraft exposed to the turbulence field; the strips on the wing and the horizontal tail are illustrated.

For the four control surfaces, the distributed force $f_{u,i}$ on the ith strip is a function of $V_{a,i}$, u and the local derivatives of lift with respect to u, which is denoted as $C_{L_{u,i}}$. The resultant forces and moments are

$$F_{a_u}u = \sum_i f_{u,i}, \quad M_{a_u}u = \sum_i r_i \times f_{u,i}$$

For the strips on the kth aerodynamic surface, the distributed force $f_{a,i}$ depends on the local airspeed $V_{a,i}$ and the local aerodynamic coefficients. The resultant forces and moments are

$$F_a = \sum_i f_{a,i}, \quad M_a = \sum_i r_i \times f_{a,i}$$

B. Flight Control Design

Using Eq. (65), Eq. (64) can be rewritten in the form of $\dot{x} = f(x) + G(x)u + d$ as

$$\begin{bmatrix} \dot{V}_f \\ \dot{\omega} \end{bmatrix} = \begin{bmatrix} -\omega \times V_f + \frac{1}{m}(F_a(V_f, \omega, 0) + F_T + F_G) \\ -J^{-1}\omega \times J\omega + J^{-1}M_a(V_f, \omega, 0) \end{bmatrix}$$
$$+ \begin{bmatrix} \frac{1}{m}F_{a_u} \\ J^{-1}M_{a_u} \end{bmatrix} u + \begin{bmatrix} \frac{1}{m}(F_a(V_f, \omega, V_w) - F_a(V_f, \omega, 0)) \\ J^{-1}(M_a(V_f, \omega, V_w) - M_a(V_f, \omega, 0)) \end{bmatrix}$$
$$(66)$$

where the aerodynamic influences of turbulence are lumped in the disturbance vector d. Consider an output tracking problem, and choose $y = Hx = [V_z, p, q, r]^T$, where H is a Boolean selection matrix. Based on Eq. (5), the vector relative degree of this system equals $\rho = [1, 1, 1, 1]^T$, $\alpha(x) = Hf(x)$, $\mathcal{B}(x) = HG(x)$. According to Eq. (21), the external states vector $\xi = y$. There are also two-dimensional internal dynamics in this application case. Although the input-to-state stability of the internal dynamics is not easy to prove, the analysis of the origin stability of $f_d(\eta, 0, 0)$ is practical. The two-dimensional submanifold for the zero dynamics is given by

$$Z^* = \left\{ x \in \mathbb{R}^6, V_z - V_z^* = p = q = r = 0 \right\} \quad (67)$$

where V_z^* is the vertical velocity in trim condition. Define
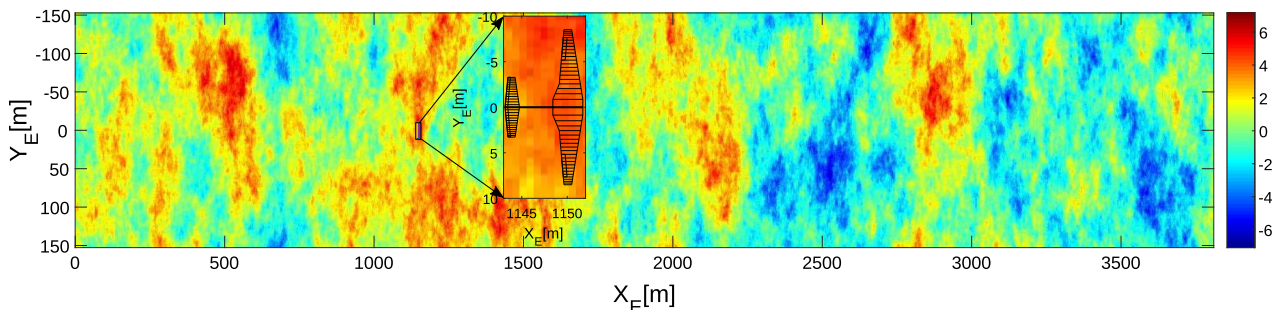

Fig. 1 Two-dimensional von Kármán vertical turbulence field with $L_g = 762$ m, $\sigma = 3$ m/s.
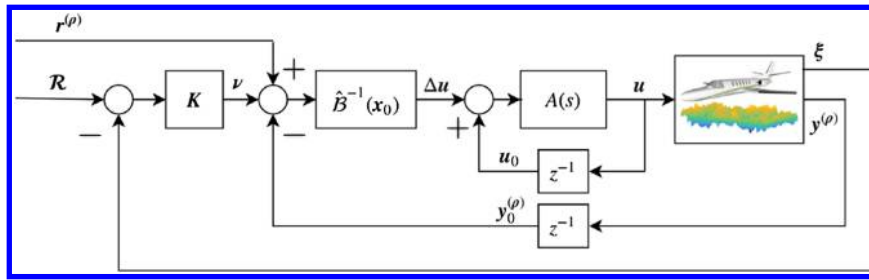
Fig. 2   Block diagram for a reference tracking problem applied considering actuator dynamics.

$$A(t) = \frac{\partial f_d}{\partial \eta}\bigg|_{\eta=0}$$

then $\eta = 0$ is an exponentially stable equilibrium point of f_d if and only if it is an exponentially stable equilibrium point of the linear system $\dot{\eta} = A(t)\eta$ [2]. This allows the origin stability of the zero dynamics to be easily tested via linearization. The origin of $\dot{\eta} = f_d(\eta, 0, 0)$ has been tested to be exponentially stable for this model.

Actuator dynamics and limits are considered in this validation. Actuators for aerodynamic control surfaces are modeled as first-order systems with transfer function $A(s) = 20/(s + 20)$. The deflection limits of ailerons, elevator, and rudder are ± 35, ± 25, ± 25 deg, respectively. The rate limit for ailerons is 100 deg/s, and it is 60 deg/s for elevator and rudder. Constant throttle δ_p^* is used in the simulations. An additional velocity controller using throttle can be designed if desired. The simulation frequency (difference from the sampling frequency) is 2000 Hz, which is chosen to be sufficiently high to simulate the property of the continuous dynamics in real life. Figure 2 illustrates a block diagram of INDI applied considering actuator dynamics.

C. Command Tracking in a Turbulence Field

This subsection considers a command tracking problem in the presence of external disturbances. During simulations, the aircraft is flying through the von Kármán turbulence field shown in Fig. 1. Symmetrical excitations are assumed in this subsection; namely, the local gust velocities $V_{w,i}$ are interpolated using the spatial locations of the right-hand side strips of the aircraft. $V_{w,i}$ of the left-hand side strips are assumed to be symmetrical to the right. Asymmetrical excitations will be considered in Sec. IV.D. Using the flight controller designed in Sec. IV.B, and referring to Corollary 1, η and the reference tracking error e can then be concluded to be ultimately bounded under small perturbations. Moreover, the ultimate bounds have been proven to be monotonically decreasing functions of K gains and the sampling frequency in Sec. III.B.1. The simulations in this subsection will test the fidelity of these conclusions when actuator dynamics and limits are considered.

Set the references for $[V_z, p, r]^T$ to be their trim values $[V_z^*, 0, 0]^T$, and the reference signal for q is designed as a sinusoid signal with amplitude of 1.5 deg/s and frequency of 1.5 rad/s. The initial errors are $e(t = 0) = [0.5$ m/s, 0 deg/s, 2 deg/s, and 0 deg/s]. Design the gain matrix as $K = a \cdot I_{4 \times 4}$, $a > 0$. In view of Fig. 2, there are three sampling processes in this control law, namely the measurement of $y_0^{(\rho)}$, ξ and the actuator position u_0. The sampling interval Δt will be varied in the subsequent analyses for testing its influences on the ultimate bounds.

In view of Figs. 3 and 4, the aircraft is able to track the pitch rate command using all sets of controller parameters. When $a = 3$, the ultimate bounds for $\Delta t = 0.01$ s are $|e_{V_z}| = 0.23$ m/s, $|e_q| = 0.30$ deg/s, which degrade into larger ultimate bounds of $|e_{V_z}| = 0.68$ m/s, $|e_q| = 0.85$ deg/s when the sampling interval increased into $\Delta t = 0.2$ s. Using the same sampling interval $\Delta t = 0.01$ s, when the outer loop gains increased from $K = 3 \cdot I_{4 \times 4}$ to $K = 8 \cdot I_{4 \times 4}$, the closed-loop system responds faster to the errors, which results in smaller ultimate bounds. The control surface deflections are illustrated by Fig. 5.
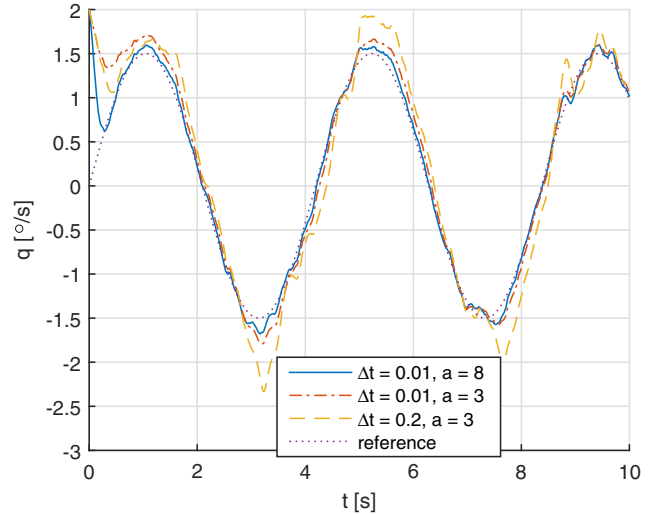

Fig. 3   Pitch rate tracking responses.

Figure 6 shows the ultimate bounds of e_{V_z} and e_q using various controller parameters. The tested sampling interval varies from $\Delta t = 0.001$ s to $\Delta t = 0.2$ s. As can be seen from Fig. 6, in general, for a given gain matrix $K = a \cdot I_{4 \times 4}$, the ultimate bounds decrease as the sampling interval decreases. This trend of decrease becomes slower around $\Delta t = 0.12$ s as the contour lines become sparser. Further decreasing the sampling interval does improve the performance but would impose higher requirements on the hardware.

On the other hand, for a given Δt, as a increases from $a = 1$ to $a = 13$, the ultimate bounds decrease first, reaching a minimum around $a \approx 8$, and then show a trend of increase as a further increases. As analyzed before, the ultimate bounds will be smaller for larger K gains when ideal actuators are applied. However, because actuators have bandwidth, rate, and position limits, high-gain control can impose unachievable commands on actuators, which consequently degrades the performance for $a > 8$ and potentially leads to divergence. High-gain control also amplifies the measurement noise in practice.

In summary, simulation results in this subsection verified the ultimate boundedness of the states under INDI control, especially when actuator dynamics and limits are considered. The influences of K gains and Δt on the ultimate bounds are also verified.

D. Robustness Comparisons with Nonlinear Dynamic Inversion

In this subsection, the robustness of the reformulated INDI control will be compared with nonlinear dynamic inversion (NDI) control, in the presence of asymmetrical turbulence excitations and model uncertainties. Equations (56) and (58) formulate the NDI and INDI control laws when the estimated models are used. Because $\xi = y = Hx$, $T_2(x) = \hat{T}_2(x) = Hx$ in Eqs. (56) and (58). During simulations, the aircraft is gradually flying through the two-dimensional (2-D) von Kármán turbulence field shown in Fig. 1, and the turbulence velocity on each aerodynamic strip is independently interpolated as $V_{w,i}$. The references for $\xi = [V_z, p, q, r]^T$ are illustrated in Fig. 7. The reference for V_z equals its trim value V_z^*.
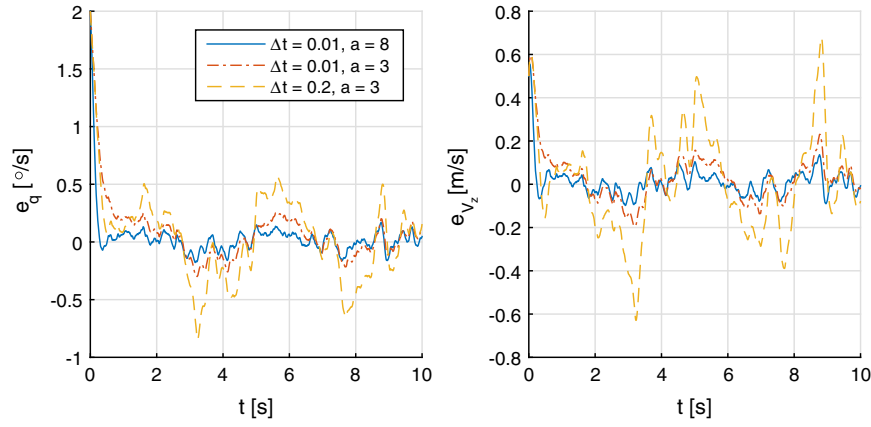
Fig. 4   Tracking error responses for pitch rate and vertical velocity.
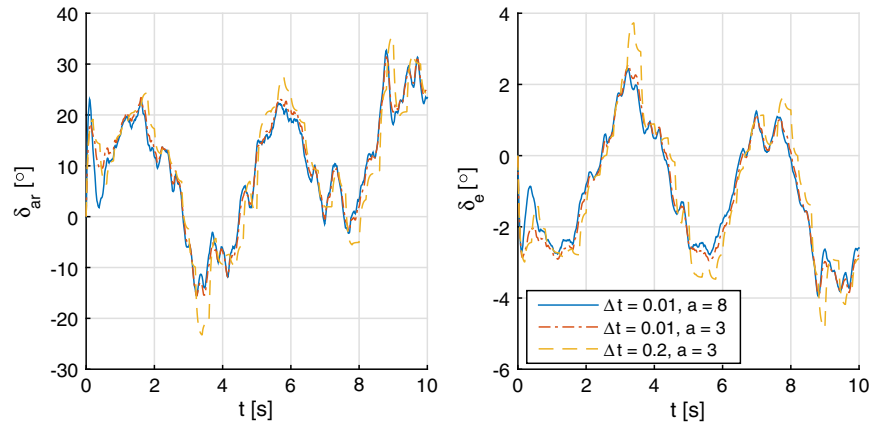

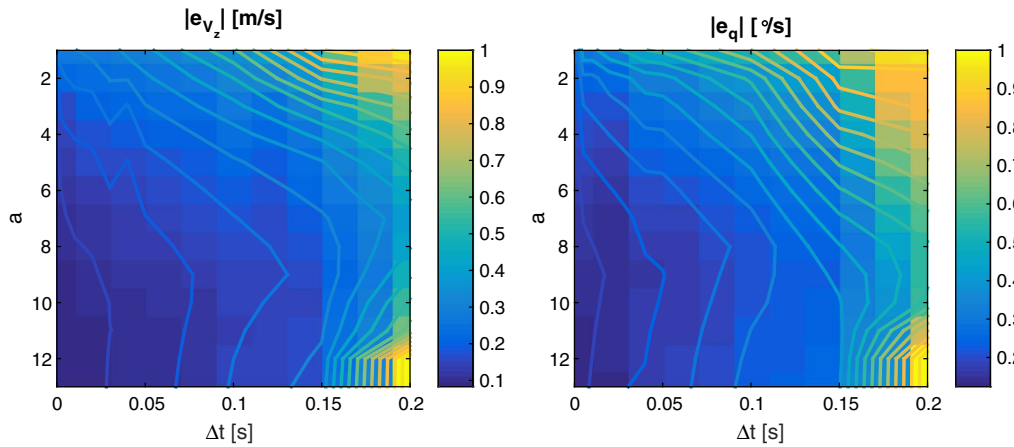Fig. 5   Control surface deflections.

Fig. 6   Influences of sampling interval and outer-loop gains on the ultimate bounds.
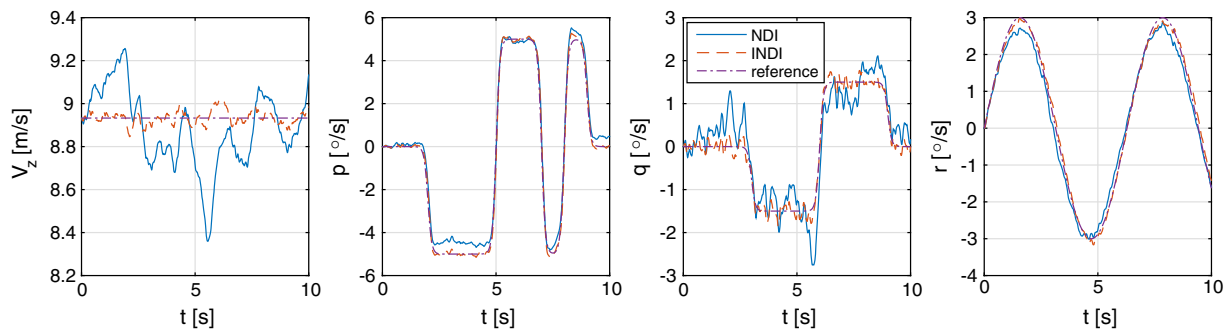

Fig. 7   Command tracking in a 2-D turbulence field.

The reference for p is a 3211 signal with magnitude of 5 deg/s realized by smoothly combined sigmoid functions. The sigmoid function $f(t) = 1/(1 + e^{-t})$ is chosen because of its differentiable property up to any order. The reference for q is a smooth realization of a doublet signal with magnitude of 1.5 deg/s. The reference for r is a sinusoid signal with magnitude of 3 deg/s and frequency of 1 rad/s. Typical testing signals are chosen as references for comparing the effectiveness of NDI and INDI. In practice, these reference signals are provided by outer-loop controllers for various flight control tasks. For example, the reference for V_z can be designed for load alleviation purposes [15], the reference for r can be designed for minimizing the side-slip angle [10], the references for p and q can be designed for the attitude tracking of ϕ and θ [7], etc. The sampling frequency used in this subsection is 100 Hz. For fair comparisons, the control gain matrices for both NDI and INDI are identical to $K = 8 \cdot I_{4 \times 4}$.

The tracking performance of NDI and INDI in the 2-D von Kármán turbulence field (Fig. 1) is compared in Figs. 7–9. Model uncertainties are not introduced in this simulation yet (i.e., $\hat{\alpha} = \alpha$, $\hat{\mathcal{B}} = \mathcal{B}$). However, the disturbance d as a function of V_w [Eq. (66)] is nonzero. Because the turbulence excitations are asymmetric, lateral states including p and r are also disturbed by d. In view of Figs. 7 and 8, aircraft using INDI control can better track the references in the turbulence field. The rms values of the tracking errors for this simulation case are summarized in the first two rows of Table 1, in which INDI shows smaller rms value of errors in all the four controlled channels. These results verify the analyses in Sec. III.B.1, in that the ultimate bounds for ξ are only influenced by the disturbance increments Δd, and the main influences of d_0 have been included in the measurements/estimations of $\dot{\xi}_0$. Figure 9 shows the control inputs, where INDI responses more actively for alleviating the turbulence influences. Moreover, the control surface deflection angles are within the limits under both NDI and INDI control.

Referring to Sec. III.B.2, when implementing the control methods, INDI control only needs the estimated control effectiveness matrix $\hat{\mathcal{B}}$, whereas NDI requires both $\hat{\alpha}$ and $\hat{\mathcal{B}}$. Recall Eq. (66); $\hat{\alpha}$ and $\hat{\mathcal{B}}$ contain the inertia and aerodynamic parameters, whose accurate estimations are very difficult to obtain in practice. Herein, the robustness of NDI
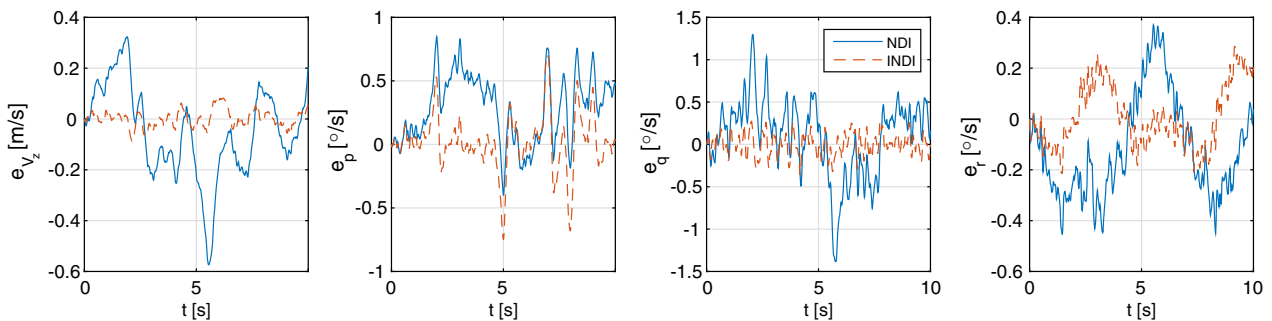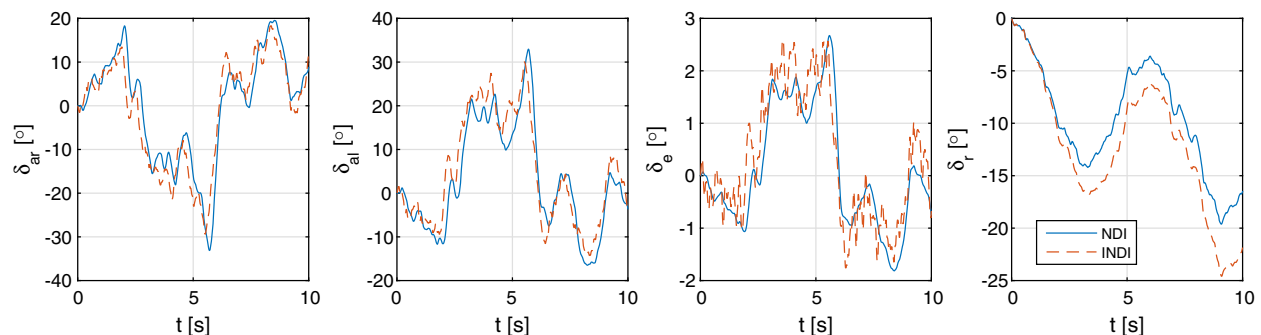
and INDI to model uncertainties will be compared. Figures 10–12 present the reference tracking responses of the aircraft in the turbulence field (Fig. 1). The estimated model $\hat{\mathcal{B}} = 1.3\mathcal{B}$ is used by both NDI and INDI. In other words, both controllers overestimate the control effectiveness matrix by 30%. On the other hand, the perfect model $\hat{\alpha} = \alpha$ is used by NDI; even so, the tracking performance of NDI is still inferior to INDI, as presented in Figs. 10 and 11.

The rms values of the tracking errors in the presence of external disturbances and model uncertainties are presented in the last two rows of Table 1. It can be seen from Figs. 10 and 11 and Table 1 that INDI has better robustness than NDI. When using NDI control, the rms values of the errors in Fig. 11 are respectively increased by 71.8, 158, 21.3, and 146% as compared to errors in Fig. 8. By contrast, INDI is less influenced by the mismatches between $\hat{\mathcal{B}}$ and $\mathcal{B}$ because the rms values of the errors in Fig. 11 are increased by 42.4, 39.9, 19.2, and 14.8% as compared to errors in Fig. 8. Furthermore, Table 1 shows that, when mismatched $\hat{\mathcal{B}}$ is used, the rms values of the tracking errors under INDI control are at least three times smaller than the values under NDI control. These results verify the analyses in Sec. III.B.2. In addition, the control surface deflections are illustrated in Fig. 12, where both INDI and NDI satisfy the actuator constrains.

The results of a Monte Carlo simulation containing 1000 samples of uncertain models are presented in Fig. 13. Both aerodynamic and inertia uncertainties are added to the estimated models $\hat{\alpha}$ and $\hat{\mathcal{B}}$. As presented in Sec. IV.A, the aerodynamic model of the present aircraft is based on strip theory. Each of the six aircraft components or the four aerodynamic control surfaces contains n_k/n_p strips with local aerodynamic coefficients. Herein, the slope of lift curve uncertainties

Table 1   RMS values of the tracking errors under NDI and INDI control

Controller	rms(e_{V_z}), m/s	rms(e_p), deg/s	rms(e_q), deg/s	rms(e_r), deg/s
NDI	0.188	0.387	0.465	0.230
INDI	0.033	0.223	0.130	0.122
NDI uncertain	0.323	0.999	0.564	0.565
INDI uncertain	0.047	0.312	0.155	0.140

Fig. 8   Tracking errors in a 2-D turbulence field.

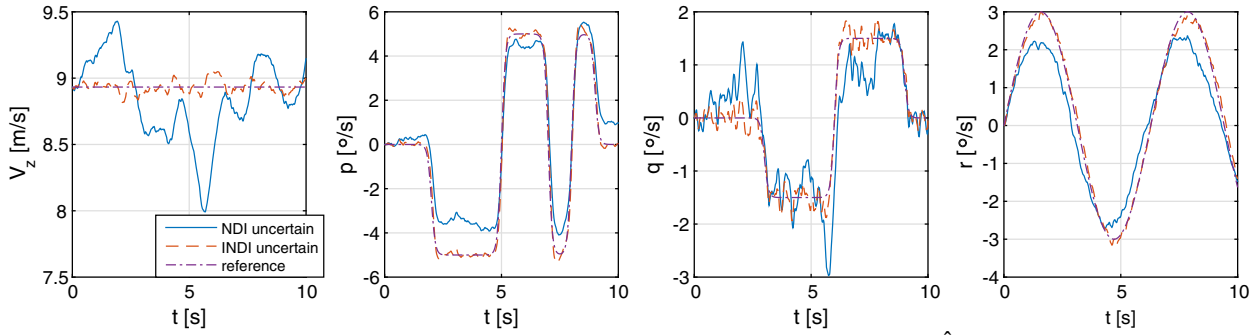**Fig. 9   Control inputs in the presence of external disturbances.**

Fig. 10   Command tracking in a 2-D turbulence field with mismatched $\hat{\mathcal{B}}$.
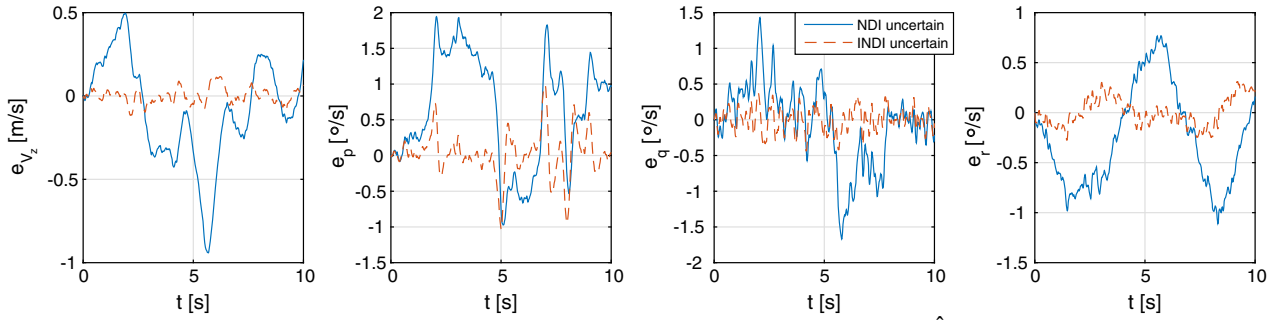

Fig. 11   Tracking errors in a 2-D turbulence field with mismatched $\hat{\mathcal{B}}$.
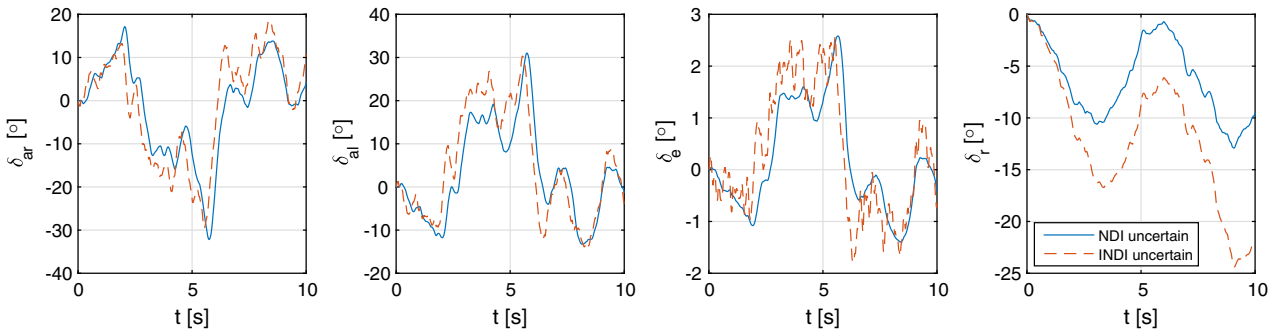

Fig. 12   Control inputs in the presence of external disturbances and model uncertainties.
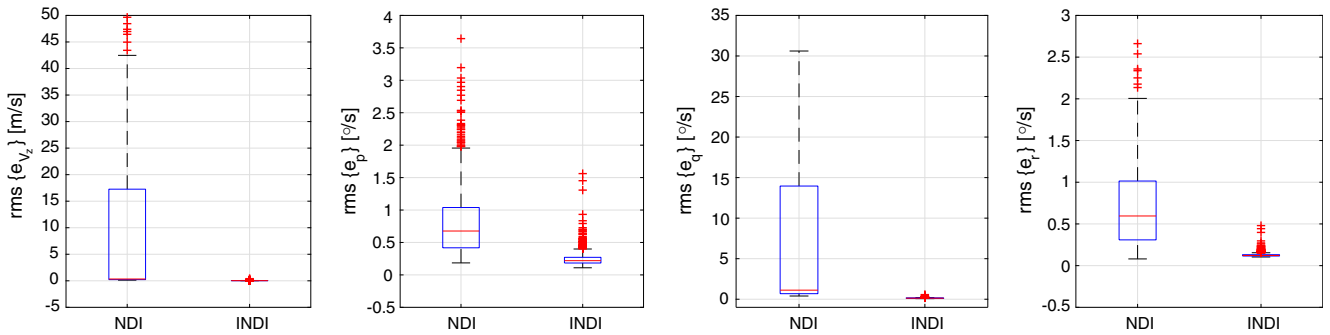

Fig. 13   Box plots of a Monte Carlo simulation for robustness comparisons between NDI and INDI.

for the kth aircraft component are modeled as normally distributed real numbers as

$$\Delta_k \sim \mathcal{N}(0, \sigma_k^2), \quad \sigma_k = \frac{0.3}{n_k} \sum_{i=1}^{i=n_k} C_{L_{\alpha,i}} \quad (68)$$

which means that, for each aircraft component k, the mean value of the slope of lift curve uncertainties equals zero, and the standard deviation σ_k is chosen as 30% of the average C_{L_α} value of this component. Analogously, for the pth aerodynamic control surface,

$$\Delta_p \sim \mathcal{N}(0, \sigma_p^2), \quad \sigma_p = \frac{0.3}{n_p} \sum_{i=1}^{i=n_p} C_{L_{u,i}} \quad (69)$$

Δ_p in the preceding equation represent the uncertainties for the derivatives of lift with respect to $\boldsymbol{u}$. The mean value of Δ_p equals zero, and the standard deviation σ_p is chosen as 30% of the average C_{L_u} value of the pth control surface. It is worth noting that this step up is more elaborate than introducing uncertainties to the conventional stability and control derivatives (e.g., C_{m_α}, C_{m_q}, C_{n_β}, C_{n_r}, $C_{m_{\delta_e}}$, $C_{n_{\delta_r}}$, etc.), by virtue of the usage of the strip theory [29]. The uncertainties

Table 2   IQR and median values of $\text{rms}(e_i)$, $i = V_z, p, q, r$ under NDI and INDI control

Control	Metrics	$\text{rms}(e_{V_z})$, m/s	$\text{rms}(e_p)$, deg/s	$\text{rms}(e_q)$, deg/s	$\text{rms}(e_r)$, deg/s
NDI	IQR $\{\text{rms}(e_i)\}$	17.04	0.621	13.27	0.706
	median $\{\text{rms}(e_i)\}$	0.339	0.677	1.119	0.595
INDI	IQR $\{\text{rms}(e_i)\}$	0.014	0.088	0.036	0.016
	median $\{\text{rms}(e_i)\}$	0.032	0.220	0.129	0.122

for mass are assumed to have normal distribution, with $\mu_m = 0$, and σ_m equals 10% of the nominal mass. Normally disturbed uncertainties are also introduced to the inertia parameters J_{xx}, J_{yy}, J_{zz}, J_{xz}. For each of the four parameters, the mean value of uncertainty equals zero, and the standard derivation is taken as 25% of the nominal inertia value.

This Monte Carlo simulation considers the command tracking task in the presence of external disturbance (Fig. 1) and model uncertainties. The references for ξ are the same as presented in Figs. 7 and 10. Simulation results with rms $\{e_{V_z}\} > 50$ m/s or max $\{\text{rms}\{e_p\}, \text{rms}\{e_q\}, \text{rms}\{e_r\}\} > 50$ deg/s are considered as the controller fails to track the commands. Among all the 1000 samples, 31 cases fail under NDI control, whereas there is no failure case under INDI control. The reason for the failure cases under NDI control can be revealed by Corollary 2 and Corollary 3 in that the ultimate boundedness of the states can only be guaranteed if ε_{ndi} is bounded. Also, when only the origin of $\dot{\eta} = f_0(\eta, 0, 0)$ is guaranteed to be exponentially stable, the uncertainties that NDI can sustain are limited, i.e., $\bar{\varepsilon}_{\text{ndi}} < \varepsilon^*$ (Corollary 3). However, because ε_{ndi} contains both $\alpha - \hat{\alpha}$ and $(\mathcal{B} - \hat{\mathcal{B}}^{-1})u_{\text{ndi}}$ [Eqs. (57) and 62], it can become unbounded in severe perturbation circumstances, especially when the actuators have nonlinear constrains.

According to the analyses in Sec. III.B.2, even for the cases that ε_{ndi} is bounded, the norm value of ε_{ndi} is still larger than that of $\varepsilon_{\text{indi}}$. As a consequence, the states under NDI control also have larger ultimate bounds in the presence of perturbations. This is verified by the box plots in Fig. 13, in which the 31 failure cases under NDI control have been discarded. The interquartile range (IQR) values and the medians of $\text{rms}(e_i)$, $i = V_z$, p, q, r are summarized in Table 2. It can be seen from Fig. 13 and Table 2 that the robust performance of NDI is significantly degraded by ε_{ndi} [Eq. (57)]. By contrast, INDI is more robust to model uncertainties and disturbances because IQR $\{\text{rms}(e_i)\}$ using INDI control are at least one order of magnitude smaller than that under NDI control for all $i = V_z, p, q, r$. Furthermore, the median values of $\text{rms}(e_i)$ under INDI control are at least three times smaller than that using NDI control, for all $i = V_z$, p, q, r.

V. Conclusions

This paper reformulates the incremental nonlinear dynamic inversion (INDI) control without using the time scale separation principle and generalizes it for systems with arbitrary relative degree. Using Lyapunov methods and nonlinear system perturbation theory, the state of the closed-loop system is proved to be ultimately bounded by a class $\mathcal{K}$ function of the perturbation bounds. There is no restriction on the perturbation value and the initial condition if the internal dynamics are input-to-state stable. Otherwise, corresponding restrictions are needed. Disturbances are shown to directly perturb the internal dynamics while perturbing the external dynamics only by their increments, which contributes to the better disturbance rejection capability of the INDI method. Moreover, INDI is shown to be more robust to regular perturbations than nonlinear dynamic inversion (NDI), without using any additional robust or adaptive techniques. It can also resist certain regions of singular perturbations. Finally, numerical comparisons with NDI and a Monte Carlo simulation demonstrate the effectiveness of the reformulated INDI control, even in the presence of model uncertainties and external disturbances.

References

[1] Slotine, J.-J. E., and Li, W., *Applied Nonlinear Control*, Prentice–Hall, Englewood Cliffs, NJ, 1991, pp. 207–271.

[2] Khalil, H. K., *Nonlinear Systems*, Prentice–Hall, Englewood Cliffs, NJ, 2002, Chaps. 4, 9, 11, 13.

[3] Reiner, J., Balas, G. J., and Garrard, W. L., "Flight Control Design Using Robust Dynamic Inversion and Time-Scale Separation," *Automatica*, Vol. 32, No. 11, 1996, pp. 1493–1504.
doi:10.1016/S0005-1098(96)00101-X

[4] Lee, H., Reiman, S., Dillon, C., and Youssef, H., "Robust Nonlinear Dynamic Inversion Control for a Hypersonic Cruise Vehicle," *AIAA Guidance, Navigation, and Control Conference and Exhibit*, AIAA Paper 2007-6685, 2007.
doi:10.2514/6.2007-6685

[5] Hodel, A., Whorton, M., and Zhu, J., "Stability Metrics for Simulation and Flight-Software Assessment and Monitoring of Adaptive Control Assist Compensators," *AIAA Guidance, Navigation and Control Conference and Exhibit*, AIAA Paper 2008-7005, 2008.
doi:10.2514/6.2008-7005

[6] Lombaerts, T., "Fault Tolerant Flight Control, A Physical Model Approach," Ph.D. Thesis, Delft Univ. of Technology, Delft, The Netherlands, 2010.

[7] Lu, P., van Kampen, E., de Visser, C., and Chu, Q., "Aircraft Fault-Tolerant Trajectory Control Using Incremental Nonlinear Dynamic Inversion," *Control Engineering Practice*, Vol. 57, Dec. 2016, pp. 126–141.
doi:10.1016/j.conengprac.2016.09.010

[8] Smith, P., "A Simplified Approach to Nonlinear Dynamic Inversion Based Flight Control," *23rd Atmospheric Flight Mechanics Conference*, AIAA Paper 1998-4461, 1998.
doi:10.2514/6.1998-4461.

[9] Bacon, B., Ostroff, A., and Joshi, S., "Reconfigurable NDI Controller Using Inertial Sensor Failure Detection & Isolation," *IEEE Transactions on Aerospace and Electronic Systems*, Vol. 37, No. 4, 2001, pp. 1373–1383.
doi:10.1109/7.976972

[10] Sieberling, S., Chu, Q. P., and Mulder, J. A., "Robust Flight Control Using Incremental Nonlinear Dynamic Inversion and Angular Acceleration Prediction," *Journal of Guidance, Control, and Dynamics*, Vol. 33, No. 6, 2010, pp. 1732–1742.
doi:10.2514/1.49978

[11] Simplício, P., Pavel, M., van Kampen, E., and Chu, Q., "An Acceleration Measurements-Based Approach for Helicopter Nonlinear Flight Control Using Incremental Nonlinear Dynamic Inversion," *Control Engineering Practice*, Vol. 21, No. 8, 2013, pp. 1065–1077.
doi:10.1016/j.conengprac.2013.03.009

[12] Acquatella, P., Falkena, W., van Kampen, E., and Chu, Q. P., "Robust Nonlinear Spacecraft Attitude Control Using Incremental Nonlinear Dynamic Inversion," *AIAA Guidance, Navigation, and Control Conference*, AIAA Paper 2012-4623, 2012, pp. 1–20.
doi:10.2514/6.2012-4623

[13] Smeur, E. J. J., Chu, Q. P., and de Croon, G. C. H. E., "Adaptive Incremental Nonlinear Dynamic Inversion for Attitude Control of Micro Air Vehicles," *Journal of Guidance, Control, and Dynamics*, Vol. 39, No. 3, 2016, pp. 450–461.
doi:10.2514/1.G001490

[14] Smeur, E. J., de Croon, G. C., and Chu, Q., "Gust Disturbance Alleviation with Incremental Nonlinear Dynamic Inversion," *2016 IEEE/RSJ International Conference on Intelligent Robots and Systems (IROS)*, IEEE Publ., Piscataway, NJ, 2016, pp. 5626–5631.
doi:10.1109/IROS.2016.7759827.

[15] Wang, X., Van Kampen, E., and Chu, Q. P., "Gust Load Alleviation and Ride Quality Improvement with Incremental Nonlinear Dynamic Inversion," *AIAA Atmospheric Flight Mechanics Conference*, AIAA Paper 2017-1400, 2017.
doi:10.2514/6.2017-1400

[16] Huang, Y., Pool, D. M., Stroosma, O., Chu, Q. P., and Mulder, M., "A Review of Control Schemes for Hydraulic Stewart Platform Flight

Simulator Motion Systems," *AIAA Modeling and Simulation Technologies Conference*, AIAA Paper 2016-1436, 2016.
doi:10.2514/6.2016-1436

[17] Huang, Y., Pool, D., Stroosma, O., and Chu, Q., "Incremental Nonlinear Dynamic Inversion Control for Hydraulic Hexapod Flight Simulator Motion Systems," *IFAC-PapersOnLine*, Vol. 50, No. 1, 2017, pp. 4294–4299.
doi:10.1016/j.ifacol.2017.08.837

[18] Grondman, F., Looye, G., Kuchar, R. O., Chu, Q. P., and Van Kampen, E., "Design and Flight Testing of Incremental Nonlinear Dynamic Inversion-Based Control Laws for a Passenger Aircraft," *2018 AIAA Guidance, Navigation, and Control Conference*, AIAA Paper 2018-0385, 2018.
doi:10.2514/6.2018-0385

[19] Matamoros, I., and de Visser, C. C., "Incremental Nonlinear Control Allocation for a Tailless Aircraft with Innovative Control Effectors," *2018 AIAA Guidance, Navigation, and Control Conference*, AIAA Paper 2018-1116, 2018.
doi:10.2514/6.2018-1116

[20] van Ekeren, W., Looye, G., Kuchar, R. O., Chu, Q. P., and Van Kampen, E., "Design, Implementation and Flight-Tests of Incremental Nonlinear Flight Control Methods," *2018 AIAA Guidance, Navigation, and Control Conference*, AIAA Paper 2018-0384, 2018.
doi:10.2514/6.2018-0384

[21] Wang, X., Van Kampen, E., De Breuker, R., and Chu, Q. P., "Flexible Aircraft Gust Load Alleviation with Incremental Nonlinear Dynamic Inversion," *2018 AIAA Atmospheric Flight Mechanics Conference*, AIAA Paper 2018-0774, 2018.
doi:10.2514/6.2018-0774

[22] Wang, X., van Kampen, E., Chu, Q., and Lu, P., "Incremental Sliding-Mode Fault-Tolerant Flight Control," *Journal of Guidance, Control, and Dynamics*, Vol. 42, No. 2, 2019, pp. 244–259.
doi:10.2514/1.G003497

[23] Cakiroglu, C., Van Kampen, E., and Chu, Q. P., "Robust Incremental Nonlinear Dynamic Inversion Control Using Angular Accelerometer Feedback," *2018 AIAA Guidance, Navigation, and Control Conference*, AIAA Paper 2018-1128, 2018.
doi:10.2514/6.2018-1128

[24] Fradkov, A. L., Miroshnik, I. V., and Nikiforov, V. O., *Nonlinear and Adaptive Control of Complex Systems*, Vol. 491, Springer, Dordrecht, The Netherlands, 1999, Chap. 1.
doi:10.1007/978-94-015-9261-1

[25] Isidori, A., *Nonlinear Control Systems*, 3rd ed., Springer–Verlag, Berlin, 1995, pp. 105–135.

[26] Yang, X., and Zhu, J. J., "Singular Perturbation Margin and Generalised Gain Margin for Nonlinear Time-Invariant Systems," *International Journal of Control*, Vol. 89, No. 3, 2016, pp. 451–468.
doi:10.1080/00207179.2015.1079738

[27] Lu, P., Van Kampen, E., and Chu, Q., "Robustness and Tuning of Incremental Backstepping Approach," *AIAA Guidance, Navigation, and Control Conference*, AIAA Paper 2015-1762, 2015.
doi:10.2514/6.2015-1762

[28] Meirovitch, L., and Tuzcu, I., "Integrated Approach to the Dynamics and Control of Maneuvering Flexible Aircraft," NASA CR-2003-211748, 2003.

[29] Wright, J., and Cooper, J., *Introduction to Aircraft Aeroelasticity and Loads*, Wiley, Chichester, England, U.K., 2007, pp. 78–81.
doi:10.2514/4.479359

[30] Etkin, B., "Turbulent Wind and Its Effect on Flight," *Journal of Aircraft*, Vol. 18, No. 5, 1981, pp. 327–345.
doi:10.2514/3.57498

[31] Etkin, B., *Dynamics of Atmospheric Flight*, Dover, Mineola, NY, 2005, pp. 215, 989.
doi:10.1007/s13398-014-0173-7.2

This article has been cited by:

1. Tuo Han, Qinglei Hu, Hyo-Sang Shin, Antonios Tsourdos, Ming Xin. 2022. Incremental Twisting Fault Tolerant Control for Hypersonic Vehicles With Partial Model Knowledge. *IEEE Transactions on Industrial Informatics* **18**:2, 1050-1060. [Crossref]

2. Daniel Milz, Gertjan Looye. Tilt-Wing Control Design for a Unified Control Concept . [Abstract] [PDF] [PDF Plus]

3. Jing Chang, Roeland De Breuker, Xuerui Wang. Discrete-time Design and Stability Analysis for Nonlinear Incremental Fault-tolerant Flight Control . [Abstract] [PDF] [PDF Plus]

4. Yagiz Kumtepe, Tijmen Pollack, Erik-Jan Van Kampen. Flight Control Law Design using Hybrid Incremental Nonlinear Dynamic Inversion . [Abstract] [PDF] [PDF Plus]

5. Paul Acquatella, Erik-Jan Van Kampen, Qi P. Chu. A Sampled-Data Form of Incremental Nonlinear Dynamic Inversion for Spacecraft Attitude Control . [Abstract] [PDF] [PDF Plus]

6. Beau Smit, Tijmen Pollack, Erik-Jan Van Kampen. Adaptive Incremental Nonlinear Dynamic Inversion Flight Control for Consistent Handling Qualities . [Abstract] [PDF] [PDF Plus]

7. Tijmen Pollack, Erik-Jan Van Kampen. Robust Stability and Performance Analysis of Incremental Dynamic Inversion-based Flight Control Laws . [Abstract] [PDF] [PDF Plus]

8. Fei Luo, Junhong Zhang, Biao Jiang. Robustness Analysis of Two Advanced Flight Control Laws: NDI and INDI 660-668. [Crossref]

9. Huihui Cheng, Shiqian Liu, Xinjian Ma, Xinhong Xie. Incremental Nonlinear Dynamic Inversion Based Fault Tolerant Control for Pilot Error and Actuator Faults 2789-2800. [Crossref]

10. Renwei Zuo, Yinghui Li, Maolong Lv, Zongcheng Liu, Zehong Dong. 2022. Design of singularity-free fixed-time fault-tolerant control for HFVs with guaranteed asymmetric time-varying flight state constraints. *Aerospace Science and Technology* **120**, 107270. [Crossref]

11. Xuerui Wang, Tigran Mkhoyan, Roeland De Breuker. 2022. Nonlinear Incremental Control for Flexible Aircraft Trajectory Tracking and Load Alleviation. *Journal of Guidance, Control, and Dynamics* **45**:1, 39-57. [Abstract] [Full Text] [PDF] [PDF Plus]

12. Muhammad Sohail Khan Raja, Qasim Ali. 2021. Recent advances in active fault tolerant flight control systems. *Proceedings of the Institution of Mechanical Engineers, Part G: Journal of Aerospace Engineering* **35**, 095441002110628. [Crossref]

13. Yu Li, Xiaoxiong Liu, Peng Lu, Qizhi He, Ruichen Ming, Weiguo Zhang. 2021. Angular acceleration estimation-based incremental nonlinear dynamic inversion for robust flight control. *Control Engineering Practice* **117**, 104938. [Crossref]

14. Balaji Jayaraman, Ajoy Kanti Ghosh. Cascaded and Non-Cascaded Incremental Nonlinear Dynamic Inversion Flight Control Applied to a Light Aircraft 189-194. [Crossref]

15. Taotao Liang, Qiaozhi Yin, Xiaohui Wei. 2021. Straight-line path-following control for roll-out phase of the equipped-skid aircraft. *Proceedings of the Institution of Mechanical Engineers, Part G: Journal of Aerospace Engineering* **57**, 095441002110501. [Crossref]

16. Quanmin Zhu, Ruobing Li, Xinggang Yan. 2021. U-model-based double sliding mode control (U DSM -control) of nonlinear dynamic systems. *International Journal of Systems Science* **2020**, 1-17. [Crossref]

17. Rafael A. Cordeiro, Jose R. Azinheira, Alexandra Moutinho. 2021. Robustness of Incremental Backstepping Flight Controllers: The Boeing 747 Case Study. *IEEE Transactions on Aerospace and Electronic Systems* **57**:5, 3492-3505. [Crossref]

18. Ye Zhou, Hann Woei Ho, Qiping Chu. 2021. Extended incremental nonlinear dynamic inversion for optical flow control of micro air vehicles. *Aerospace Science and Technology* **116**, 106889. [Crossref]

19. Xuerui Wang, Tigran Mkhoyan, Iren Mkhoyan, Roeland De Breuker. 2021. Seamless Active Morphing Wing Simultaneous Gust and Maneuver Load Alleviation. *Journal of Guidance, Control, and Dynamics* **44**:9, 1649-1662. [Abstract] [Full Text] [PDF] [PDF Plus]

20. Ole Pfeifle, Walter Fichter. 2021. Cascaded Incremental Nonlinear Dynamic Inversion for Three-Dimensional Spline-Tracking with Wind Compensation. *Journal of Guidance, Control, and Dynamics* **44**:8, 1559-1571. [Citation] [Full Text] [PDF] [PDF Plus]

21. Zhihao Cai, Zexin Wang, Jiang Zhao, Yingxun Wang. 2021. Equivalence of LADRC and INDI controllers for improvement of LADRC in practical applications. *ISA Transactions* **53**. . [Crossref]

22. Wenqiang Zu, Hongyu Yang, Renyu Liu, Yulong Ji. 2021. A Multi-Dimensional Goal Aircraft Guidance Approach Based on Reinforcement Learning with a Reward Shaping Algorithm. *Sensors* **21**:16, 5643. [Crossref]

23. Hemjyoti Das, Daan Pool, Erik-Jan van Kampen. Incremental Nonlinear Dynamic Inversion Control of Long-Stroke Pneumatic Actuators 978-983. [Crossref]

24. Nakash Nazeer, Xuerui Wang, Roger M. Groves. 2021. Sensing, Actuation, and Control of the SmartX Prototype Morphing Wing in the Wind Tunnel. *Actuators* **10**:6, 107. [Crossref]

25. Pan Tang, Fubiao Zhang, Tianze Zhou, Defu Lin, Yingdong Hu. Fault-Tolerant Trajectory Tracking Control of a Quadrotor Suffering a Complete Rotor Failure 5208-5213. [Crossref]

26. Bo Sun, Erik-Jan van Kampen. 2021. Intelligent adaptive optimal control using incremental model-based global dual heuristic programming subject to partial observability. *Applied Soft Computing* **103**, 107153. [Crossref]

27. Runqi Chai, Antonios Tsourdos, Al Savvaris, Senchun Chai, Yuanqing Xia, C.L. Philip Chen. 2021. Review of advanced guidance and control algorithms for space/aerospace vehicles. *Progress in Aerospace Sciences* **122**, 100696. [Crossref]

28. Byoung-Ju Jeon, Min-Guk Seo, Hyo-Sang Shin, Antonios Tsourdos. 2021. Understandings of incremental backstepping controller considering measurement delay with model uncertainty. *Aerospace Science and Technology* **109**, 106408. [Crossref]

29. Bowen Nie, Zhitao Liu, Tianhao Guo, Litao Fan, Hongxu Ma, Olivier Sename. 2021. Design and Validation of Disturbance Rejection Dynamic Inverse Control for a Tailless Aircraft in Wind Tunnel. *Applied Sciences* **11**:4, 1407. [Crossref]

30. Xuerui Wang, Tigran Mkhoyan, Roeland De Breuker. Nonlinear Incremental Control for Flexible Aircraft Trajectory Tracking and Load Alleviation . [Abstract] [PDF] [PDF Plus]

31. Erwin Mooij, Xuerui Wang. Incremental Sliding Mode Control for Aeroelastic Launch Vehicles with Propellant Slosh . [Abstract] [PDF] [PDF Plus]

32. Baoxu Jia, Liguo Sun, Yanyang Wang, Xiaoyu Liu, Weigao Dang. 2021. Switched Adaptive Sliding Mode Disturbance Observer for Nonlinear Fault-Tolerant Flight Control. *IEEE Access* **9**, 92614-92628. [Crossref]

33. Yunjie Yang, Xiangyang Wang, Jihong Zhu, Xiaming Yuan, Xiaojun Zhang. 2020. Robust proportional incremental nonlinear dynamic inversion control of a flying-wing tailsitter. *Proceedings of the Institution of Mechanical Engineers, Part G: Journal of Aerospace Engineering* **234**:16, 2274-2295. [Crossref]

34. Cao Su, Xiangke Wang, Lincheng Shen, Huangchao Yu. Adaptive UAV maneuvering control system based on dynamic inversion and long-short-term memory network 6880-6885. [Crossref]

35. Byoung-Ju Jeon, Min-Guk Seo, Hyo-Sang Shin, Antonios Tsourdos. 2020. Understandings of Classical and Incremental Backstepping Controllers With Model Uncertainties. *IEEE Transactions on Aerospace and Electronic Systems* **56**:4, 2628-2641. [Crossref]

36. Bo Sun, Erik-Jan van Kampen. 2020. Incremental model-based global dual heuristic programming with explicit analytical calculations applied to flight control. *Engineering Applications of Artificial Intelligence* **89**, 103425. [Crossref]

37. Xuerui Wang, Erik-Jan van Kampen, Qiping Chu. 2019. Quadrotor fault-tolerant incremental nonsingular terminal sliding mode control. *Aerospace Science and Technology* **95**, 105514. [Crossref]

38. Nuno Miguel Guerreiro, Alexandra Moutinho. Robust Incremental Backstepping Controller for the Attitude and Airspeed Tracking of a Commercial Airplane 607-611. [Crossref]

39. Xuerui Wang, Sihao Sun, Erik-Jan van Kampen, Qiping Chu. 2019. Quadrotor Fault Tolerant Incremental Sliding Mode Control driven by Sliding Mode Disturbance Observers. *Aerospace Science and Technology* **87**, 417-430. [Crossref]